UIDE

Powered by
Arizona State University

ING. MECATRÓNICA

Tesis previa a la obtención del título de Ingeniero en Mecatrónica.

AUTOR: Ricardo Andre Yépez Zúñiga

TUTOR: Ing. Luis Andrade, D.Sc.

Design and construction of a 4-axis Drag Knife CNC machine implemented with artificial intelligence for quality control.

Diseño y construcción de una máquina CNC de cuchillas de arrastre de 4 ejes implementada con inteligencia artificial para el control de calidad

QUITO – ECUADOR | 2023

CERTIFICATE OF AUTHORSHIP

I, Student Name, hereby declare that this submission is my own work, it has not been previously submitted for any degree or professional qualification and that the detailed bibliography has been consulted.

I transfer my intellectual property rights to the Universidad Internacional del Ecuador, to be published and divulged on the internet, according to the provisions of the Ley de Propiedad Intelectual, its regulations and other legal dispositions.

Ricardo Yépez

ACKNOWLEDGMENTS

I would like to express my heartfelt gratitude to everyone who has supported and helped me throughout the course of this project.

First and foremost, I would like to thank my project supervisor, as well as all the professors with whom I had the opportunity to learn in their subjec , for their guidance, support, and encouragement throughout the entire process. I am deeply grateful for their invaluable insights and expertise, which have helped me to complete this project to the best of my abilities.

I would also like to thank my colleagues and peers, who have provided me with valuable feedback, suggestions, and support. I appreciate the time and effort that they have invested in helping me to complete this project successfully.

I would also like to acknowledge the contributions of my family and friends, who have provided me with emotional support and encouragement throughout the course of this project. Their love and support have been a constant source of inspiration and motivation for me.

Finally, I would like to thank my funding sources, ARNEM, for their financial support, which has allowed me to complete this project and make it a reality. Without their assistance, this project would not have been possible.

Thank you all for your support and contributions. I am deeply grateful for everything that you have done to help me.

CONTENTS

LIST OF FIGURES

LIST OF TABLES

DESIGN AND MATERIALS SELECTION

1. 4-AXIS DRAG KNIFE CNC

A CNC (computer numerical control) drag knife or tangential blade with 4 axes is a machine tool that is used to cut and shape materials, such as metal, plastic, or wood. It is called a tangential blade because it has a blade that rotates in a circular motion and can be positioned at different angles to the workpiece. Fig.1

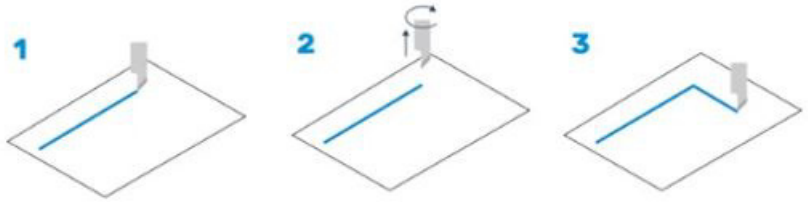

Figure 1. Rotary 4 Axis of a CNC. [1]

The 4 axes refer to the number of directions in which the blade can move. In this case, the blade can move along the X, Y, and Z axes (which are typically linear, up-and-down, left-and-right, and front-and-back movements, respectively) and also can rotate around the A axis (which is typically a rotational movement around the blade).

The CNC part of the name refers to the fact that the machine is controlled by a computer, which is programmed to move the blade in precise ways in order to create the desired shape or cut in the material. This allows for precise and automated manufacturing processes.

CNC tangential blades with 4 axes are used in a this case to cut cardboard material. They can be used to create a wide range of products depending on the geometry design, which in the paper industry are difficult to achive by a manual manufacturing way.

One of the main advantages of using a CNC tangential blade with 4 axes is the high level of precision that it offers. The computer control allows for very accurate cuts and shapes to be made, which can be difficult or even impossible to achieve using man-

ual methods. This precision can be especially important where even small variations in size or shape can have significant impacts on the functionality or safety of the final product.

Another advantage of CNC tangential blades with 4 axes is the ability to quickly and easily change between different cutting and shaping operations. Because the machine is controlled by a computer, it can be programmed to perform a wide range of tasks simply by changing the code that is used to control the blade's movements. This makes it possible to produce a wide range of products on a single machine, rather than needing multiple specialized machines for different tasks.

There are also several safety benefits to using CNC tangential blades with 4 axes. Because the machine is automated, there is less need for operators to be in close proximity to the blade while it is moving. This can help to reduce the risk of accidents or injuries on the job. Additionally, because the machine is controlled by a computer, it can be programmed to stop immediately if any problems or errors are detected, which can help to prevent damage to the machine or the workpiece.

2. Corrugated Cardboard

Corrugated cardboard is a type of paperboard that is made from three layers of paper. The inner layer, also known as the corrugate or corrugated medium, is made of wavy paper that is sandwiched between two flat outer layers, known as the liners. The corrugate is made by pressing moistened paper pulp into corrugated molds, which gives it its distinctive wavy shape. The liners are made of flat sheets of paper that are adhered to the corrugate using a type of glue or adhesive. B Flute is the type of corrugated sheet which will be used for this project, it dimension are seen in Fig. 2

Figure 2. Corrugated Cardboard. [1]

3. Mechanical Design

3.1. 4-Axis Rotary Blade

A 4 axis rotary blade is a type of cutting tool that is mounted on a machine with four axes of motion. It is typically used to cut or shape materials such as metal, plastic, or wood. The blade is mounted on a rotary spindle that can be controlled by the machine's computer numerical control (CNC) system. This allows the blade to move in multiple directions. In order to implement an adequate design for the blade, two important factors must be taken into account: the first is the angle of the cutting blade, and the second is the position offset caused by this blade. As is seen in Fig.3

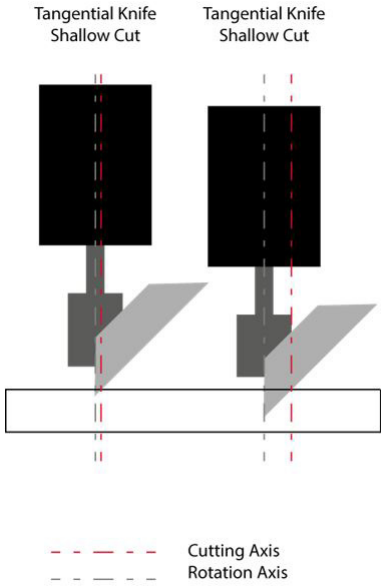

Figure 3. Blade. [1]

Tangential Blade

The angle of the blade allows knowing the depth of cut and the cutting distance of the tip with respect to the sheet, which in this case is cardboard.

In Fig.4, two cases are presented. First, where the blade has a angle of $75°$ it means the total blade´s surface which cut tangentially against the cardboard is given as:

$$Total_{cut} = \sqrt{1.09^2 + 3^2} = 3.19\ [mm] \tag{1}$$

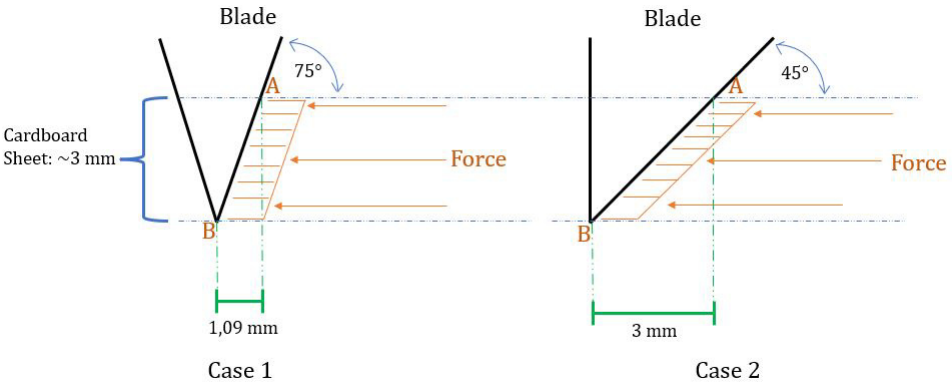

Figure 4. Types of blades.

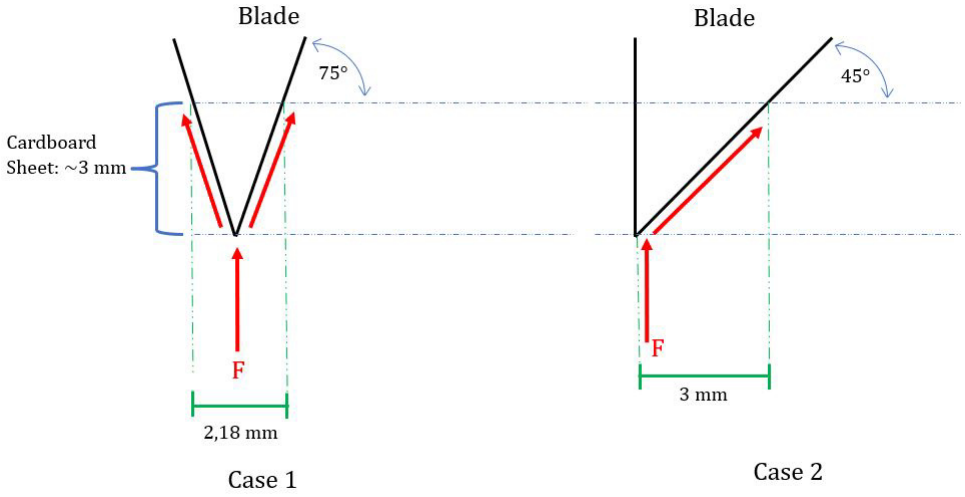

Figure 5. Types of blade: Plunge Force distribution

The second case is when the blade has an angle of $45°$:

$$Total_{cut} = \sqrt{3^2 + 3^2} = 4.24\ [mm] \tag{2}$$

Given the cases, it is observed that case two presents a greater cutting distance with the blade, this means that the cutting force will be better distributed as well ditributed along one side of the blade. Knowing the two possible cases, its cutting operation is verified by means of a simple design, as presented in the Fig. 6, 7.

Aiming at its test in the physical environment with a B flute cardboard sheet. The process consist in the measured of the required cutting force taken by a dynamometer.

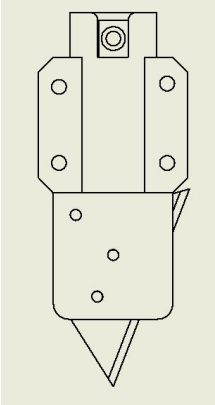

Figure 6. Blade 1 [Designed in Inventor]

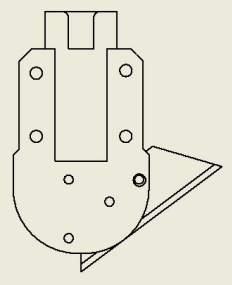

Figure 7. Blade 2 [Designed in Inventor]

A sheet of 920 mm by 920 mm was considered the total area, which is the approximate of the proposed work table. The sheet was placed on top of a shelf holding its edges like hooks to verify that it does not present any displacement when the cut is executed. In the two cases of blades, the results are show in Fig.8. The results show that the second blade design is more efficient and reduces the force necessary to enhance the cut in the sheet.

By having the blade with a more perpendicular angle, it generates a reaction in the cardboard cut that causes more force to be applied to make the cut, and if the conditions of the sheet are concave, due to the fact in this case, there were no suction, at one point of the cut the blade begins to drag material instead of cutting it, thus the blade with in case 2 has better cutting efficiency. As in the test of Fig. 9.

Finally, to reduce the coefficient of friction of the blade on its sides, the dimension of the tip was reduced by half as shown in Fig. 10.

The results of table 1 where obtained in Fig.1, considering each test structured by 4 observations of the same conditions of the blade a trajectory P0(0,0) to P1(100,100)

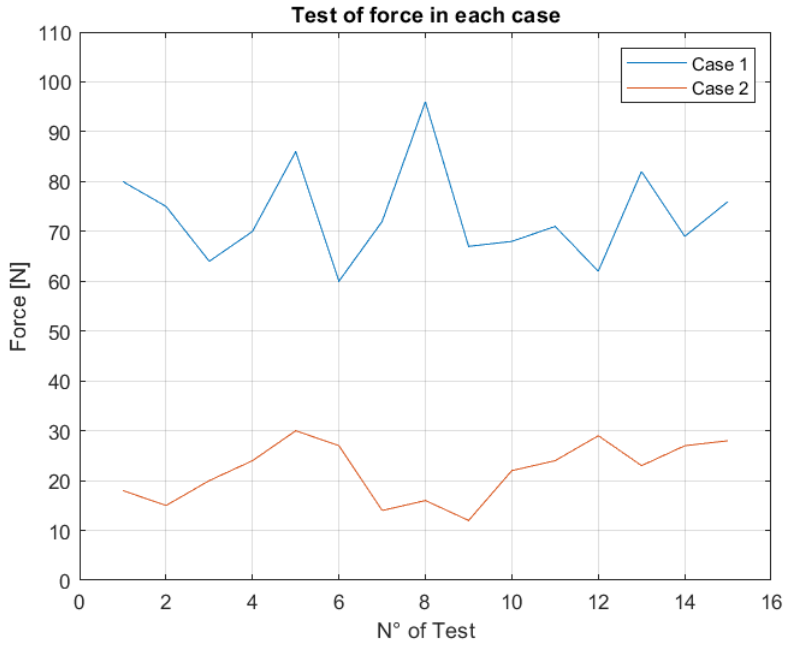

Figure 8. Force Test [Made in Matlab]

Figure 9. Blade cutting: Case 1 and 2

[mm].

In this way, it is demonstrated that the means of the observations with the chosen blade are within the limits of the relationship as well as that they remain stable in their range, according to the Fig. 11 and 12.

3.2. Suction Sytem

With the value of the force necessary to cut the sheet, this being 20.76 N. The force of the pump necessary to establish an efficient and effective suction can be estimated by setting first the conditions of the system as in Fig. 13.

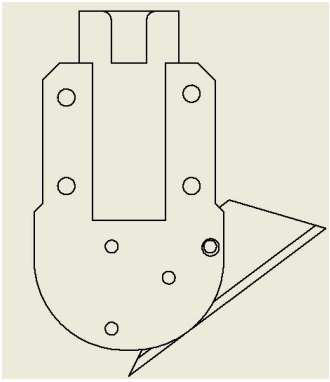

Figure 10. Blade 3 [Designed in Inventor]

Table 1. Force tests

Test N°	Ob 1 [N]	Ob 2 [N]	Ob 3 [N]	Ob 4 [N]
1	20,01	22,24	28,12	17,95
2	25,74	20,32	22,63	20,08
3	27,67	24,79	19,22	16,40
4	19,27	16,36	17,41	26,07
5	15,75	15,02	13,09	27,01
6	15,08	21,92	26,07	28,93
7	14,19	14,85	14,26	27,81
8	27,70	12,17	26,77	29,91
9	27,22	18,56	26,79	17,32
10	12,41	20,42	12,99	15,02
11	21,80	27,74	13,75	22,44
12	13,05	12,96	27,47	28,45
13	15,16	26,30	23,11	21,90
14	29,20	15,10	12,05	20,86
15	19,92	27,50	26,30	14,77
			Average cutting force:	**20.76**

where:

- Fc = required force for the cardboard´s cutting.
- Fr = opposite friction force.

$$Fc = Fr \tag{3}$$

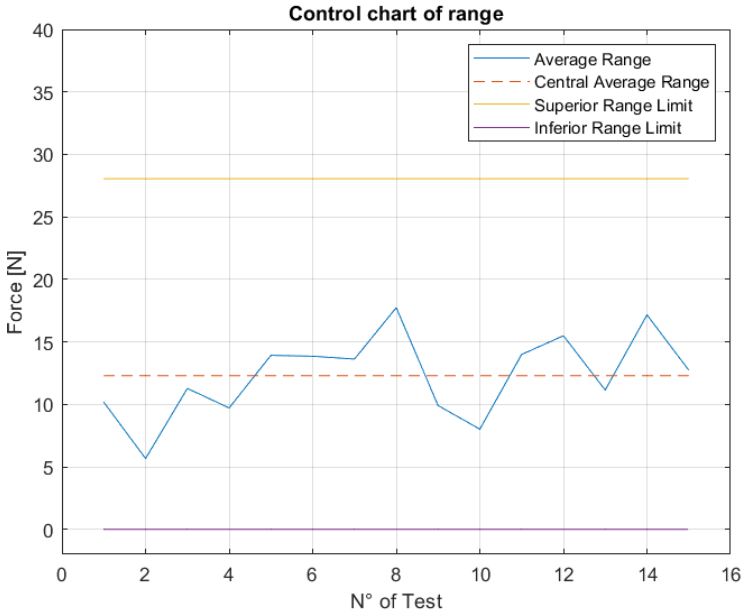

Figure 11. Control chart of range [Made in Matlab]

$$Fn = Fw \tag{4}$$

- 920x920 mm cardboard plate mass (m_l) = 0.432 kg.
- Polyteran mass of sheet 920x920x20 mm (m_p) = 0.432 kg.
- Polyteran coefficient of friction u = 3 [12].
- Gravity g = 9.81 m/s^2

Like the cardboard sheet chosen for the dimensions of the proposed base, the polyurethane sponge P7C3GW275 is chosen with the same dimensions but with a thickness of 20 mm which is the planned routed base depth. Fig. 14, which has a porosity of 95% Fig. 15.

The calculations are made by solving the suction force required to pump [13]:

$$Fn = m * g = (m_l + m_p) * g = 4.23\ N \tag{5}$$

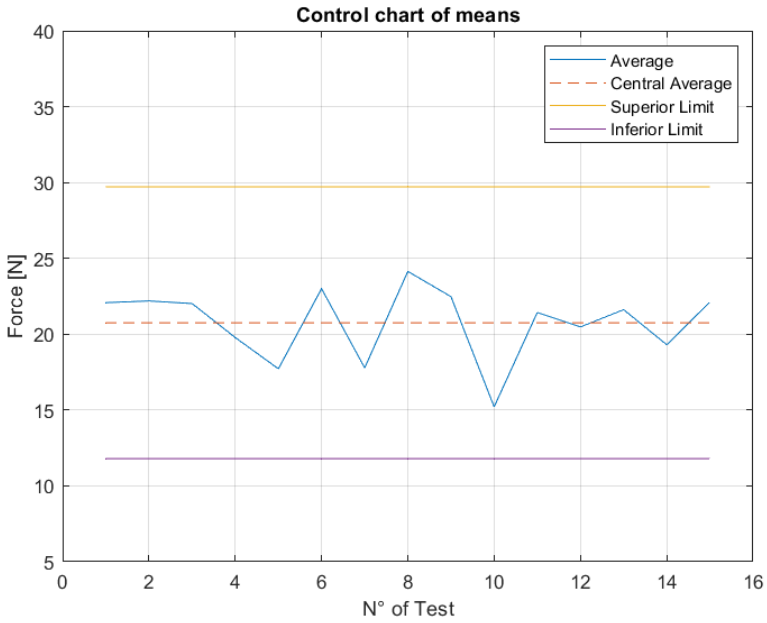

Figure 12. Control chart of means [Made in Matlab]

Determining that there must be a suction force, this will be called Fs, and it is implemented together with the sum of the normal force as an additional force:

$$Fr = u * (Fn + Fs) \tag{6}$$

$$Fs = \frac{Fc}{u} - Fn = 0.72\ N \tag{7}$$

Suction vacuums on the market have the following characteristics [14]:

- Voltage = 110 V
- Power Comsuption = 1100 W
- Speed = 1800 rpm
- Average airflow rating = 200 cfm

The data of the vacuum is used as an estimate of the vacuum speed available on the markup, giving the equation 8 and 9:

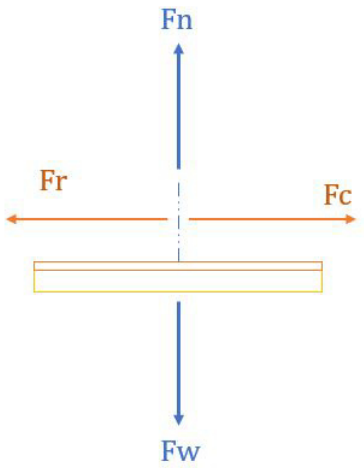

Figure 13. Force System

Figure 14. PU 12CN Foam

$$n = \frac{1800\ rev * 2 * \pi\ rad}{min * rev * 60\ sec} = 188.47\ \frac{rad}{s} \tag{8}$$

$$T = 0.72N * 1 * m = 0.72\ N * m \tag{9}$$

Then the output power is calculated with the equation 10.

$$P = 0.72N * m * 188\frac{rad}{s} = 135.37\ W \tag{10}$$

Polymer	*Density* $kg\ m^{-3}$	*Porosity* *vol-%*	*Glass Transition Temperature* $^{\circ}C$
P7C3GW275	51.5 ± 0.5	95.8	-5.1
P7C3GW200	73.4 ± 1.2	94.0	-9.8
P7C3GW125	81.2 ± 1.2	93.3	-13.31
P7C3GW050	132.5 ± 5.8	89.1	-18.67
P6C3G1LW200	76.7 ± 12.8	93.7	3.04
P7C2G1LW200	60.6 ± 3.2	95.1	-2.09

Figure 15. Foam Properties: P7C3GW275 [2]

Design and tests

By standardizing the required and available power of the suction vacuum on the market, it can be said that although a 135.73 W vacuum is needed, there is no available option on the market with these low capacities, so a price vacuum suction is chosen by standard quality-price of 1400 W as shown in Fig. 16.

Figure 16. Vacuum Pump

The safety factor for the required suction power has a value of 10.37, equation 11.

$$s.f = \frac{1400W}{135.37W} = 10.37 \tag{11}$$

On the other hand, the suction connection system was proposed as a suction divided into 2 sections, each section with 3 ports so that in this way there is an equitable suction. As shown in the Fig. 17, the connection are made with PVC pipes and in Fig 18 the number of suction holes are seen.

With the proposed design and the characteristics of the pump, it is verified by CFD computational fluid dynamics simulation in Autodesk CFD.

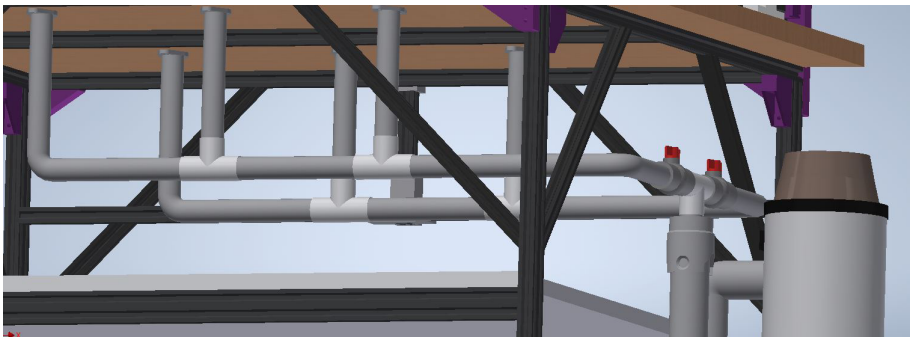

Figure 17. Connection Suction System [Designed in Inventor]

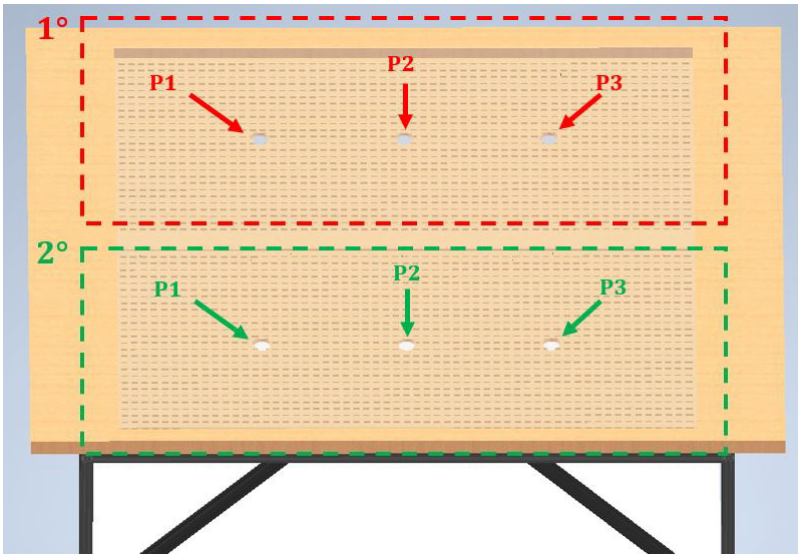

Figure 18. Vacuum Suction base [Made in Inventor]

- **CFD Conditions:** For the simulation conditions, 3 objects are placed, the PVC pipe system, the air flow object and the cardboard plate of 2 mm width (Flute E), Fig. 19.
  - Air Flow rate: Q = 200 cfm = 0.09438 m^3/s
  - Inner radius of the pipeline: r = 0.024 m

  The average velocity of the airflow is calculated with equation 12.

$$v = \frac{Q}{A} = \frac{0.09438\ \frac{m^3}{s}}{\pi * (0.024\ m)^2} = 208.625\ \frac{m}{s} \tag{12}$$

- **Suction trajectory and velocity:** Within this part, the CAD design is evaluated

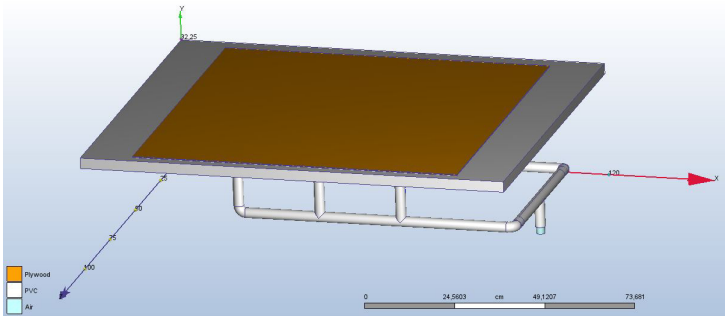

Figure 19. CFD Conditions [Made in Autodeks CFD]

based on the suction trajectory that follows the air flow through the suction system, as shown in Fig. 20.

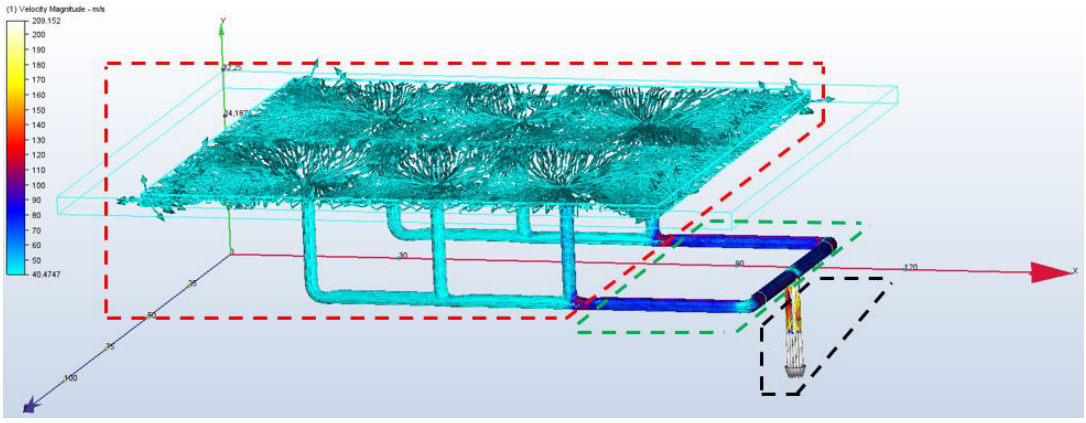

Figure 20. Suction velocity [Made in Autodeks CFD]

In Fig. 20, 3 averages of air suction speed are seen; The first one is within the red section whose speed is represented with a light blue color having an average value of 40.47 m/s, which is maintained during the entire suction base to the 3 main pipes of each section, then there is a speed with a value of 80 m/s represented with a dark blue color within the green section, the value within this section verifies that there is a sum of air flow since it is next to reach the base point of suction, and finally, the black section shows the final speed values, being this 209,152 m/s that reaches the main suction point, verifying the final flow rate of 0.09438 m^3/s of the vacuum in equation 12.

On the other hand, Fig. 21 shows the trajectory of the air flow that follows in the system, at the base it can be seen how the flow goes directly to the suction holes. An important feature to mention is that within the suction system a free suction

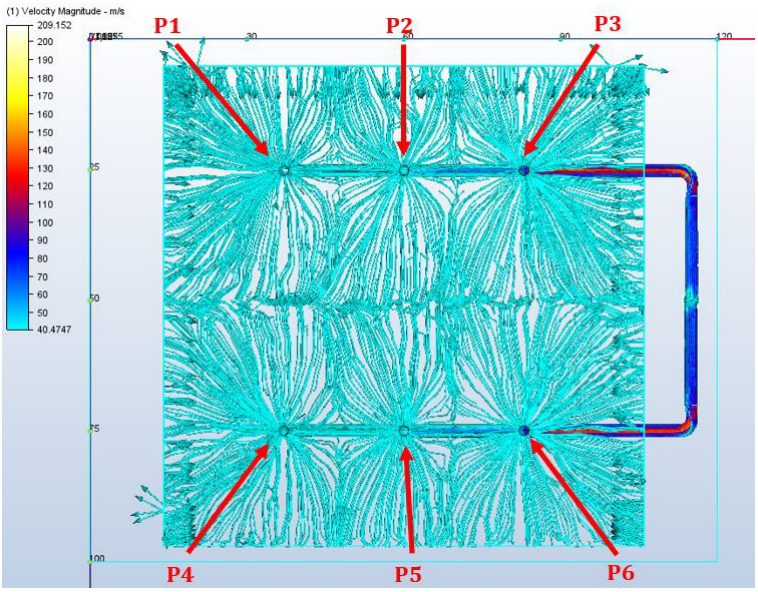

Figure 21. Suction trajectory [Made in Autodeks CFD]

opening must be proposed to prevent the pump from damaging it [15], for this reason the dimensions of the cardboard sheet are a little smaller per millimeter compared to the area of suction of the base, consequently in the simulation it is observed that in the entire profile of the base there is a flow trajectory from outside to inside.

- **Suction Force:** In this part, the average force exerted on the entire main base that must suck the E-flute cardboard sheet is evaluated.

  Fig. 22 shows that the average value of the suction force on the plate is 60 N represented with the light blue color, the main red section encloses the main section forces having peaks of up to 140 N. On the other hand, the black sections show the areas with the least applied force on the plate represented with a dark blue color with an average value of 10 N, so it can be said that the main suction forces are found in the areas closest to the holes of the suction ducts.

  Likewise, it can be seen in Fig. 23 that the suction force is downwards, demonstrating that the suction keeps the cardboard sheet fixed against the main base as shown in the real system represented in Fig. 19.

To determine the average force for the safety factor, the same procedure must be carried out as in the equation 6, but this time considering the average suction force of 60 N

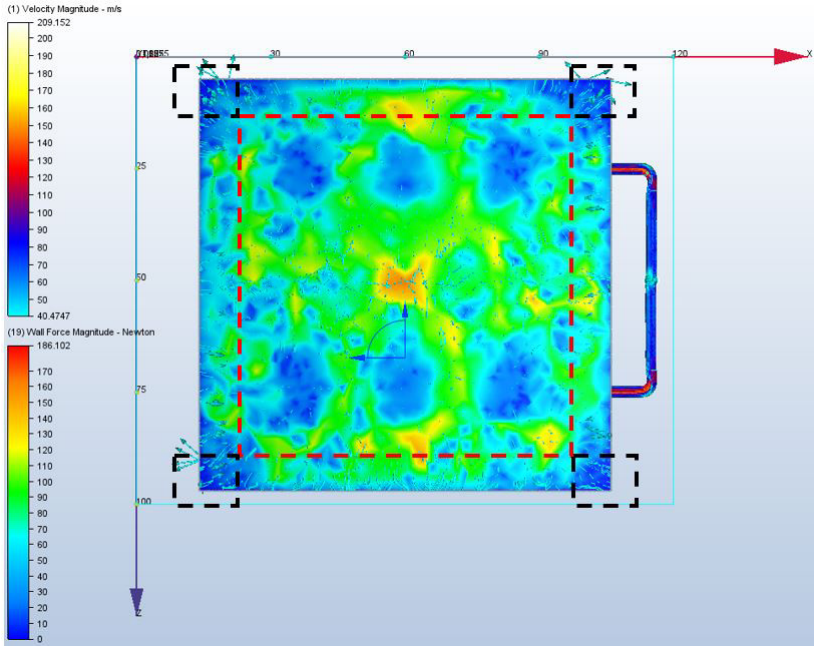

Figure 22. Suction Force [Made in Autodeks CFD]

the system must have to ensure the fixing of the plate to later determine the maximum limit cutting force necessary for the plate to move during the manufacturing process of the box simulating an offset as a manufacturing error of the CNC, establishing this force as the maximum cutting force that must be applied in the CNC. The equation 13 shows the process.

$$Fc_{max} = Fr = u * (Fn + Fs) = 3 * (4.23\ N + 60\ N) = 192.69\ N \tag{13}$$

Once the vacuum has been acquired, sizing tests are carried out. For this test, a dynamometer was used to measure the force necessary to move the cardboard sheet horizontally and move it a few millimeters only to change its position for a couple centimeter, enough to simulate it as error, as shown in Fig. 24.

If the plate moves, it means that the necessary force has been reached to overcome the suction force of the system. Table 2.

In this way, it is established that the force necessary to move the cardboard plate when the suction system is on, is 195.53 N as maximum cutting force, as it was also verified in the simulation result calculated in equation 13 then it can be demostrated, equation

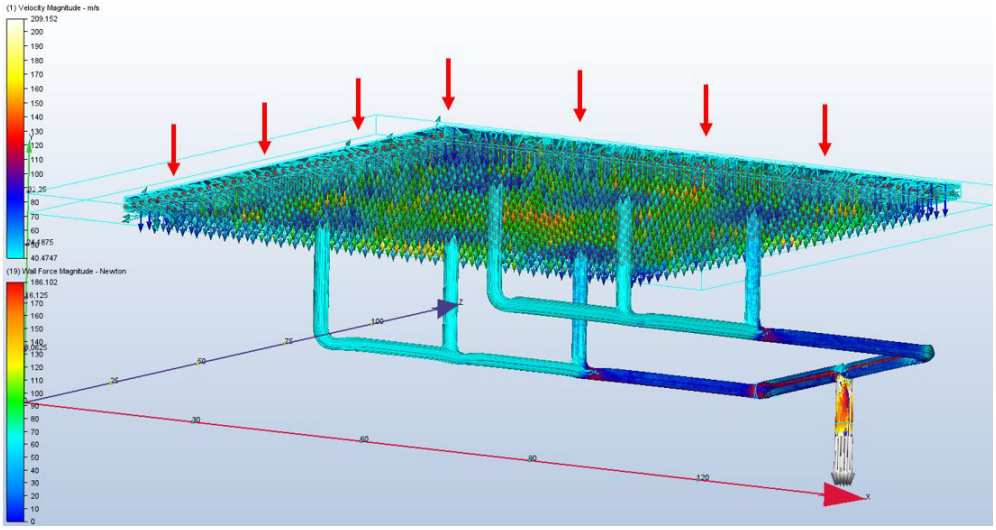

Figure 23. Suction Force Direction [Made in Autodeks CFD]

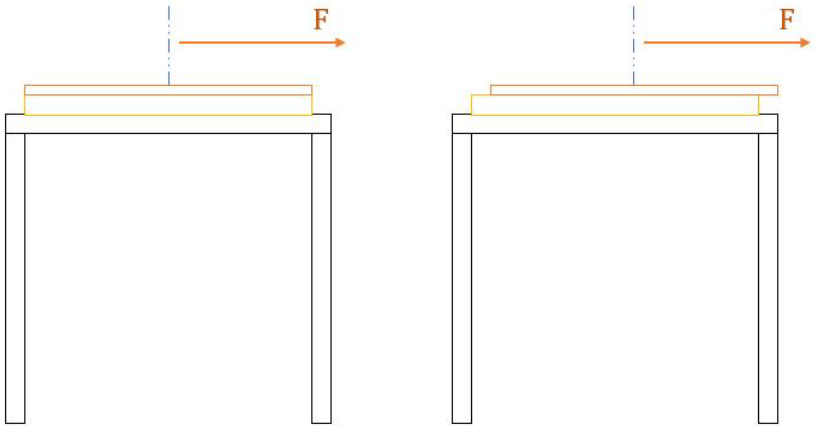

Figure 24. Suction Test

14:

$$Average\ cutting\ force < Maximum\ cutting\ force \tag{14}$$

$$20.76\ N < 195.53\ N \tag{15}$$

Consequently, the safety factor is calculated in equation 16:

Table 2. Force test with suction system

Test	Force [N]
1	196,2
2	200,3
3	185,8
4	193,6
5	197
6	195,8
7	197,7
8	195,4
9	197,5
10	196
Mean:	**195,53**

$$ns = \frac{195.53N}{20.76N} = 9.41 \tag{16}$$

Resulting a value of safety factor of 9.41 for the cutting force to be applied in CNC avoiding any displacement to be translated in the machine as an offset in the coordinates and not correctly verifiyng the path to ensure the correct dimensions of the final product.

3.3. Aluminium V-Slot profile

V-Slot or T-slot profiles of type rosch rexroth are high-quality, open-source aluminum linear rail profiles with a V- or T-slot on the sides of the profile. It's accurate, easy to use, and allows you unlimited design control through its modular nature. Within this design, the type of V-slot profile is considered for the CNC´s structure due to its V-slot for bearings with linear movement directly without rails. These profiles are made of 6063 T5 aluminum with the following properties:

Table 3. Aluminium 6063 T5

Physical Properties	Value	Unit
Ultimate Tensile Strength	186	MPa
Tensile Yield Strength	145	MPa
Modulus of Elasticity	68.9	GPa
Poisson's Ratio	0.33	-
Shear Modulus	25.8	GPa

Source: 6063 T5 Series Aluminum Alloy [16]

3.4. Z and X Mechanism

Z-Axis

The proposed design is shown in Fig. 25

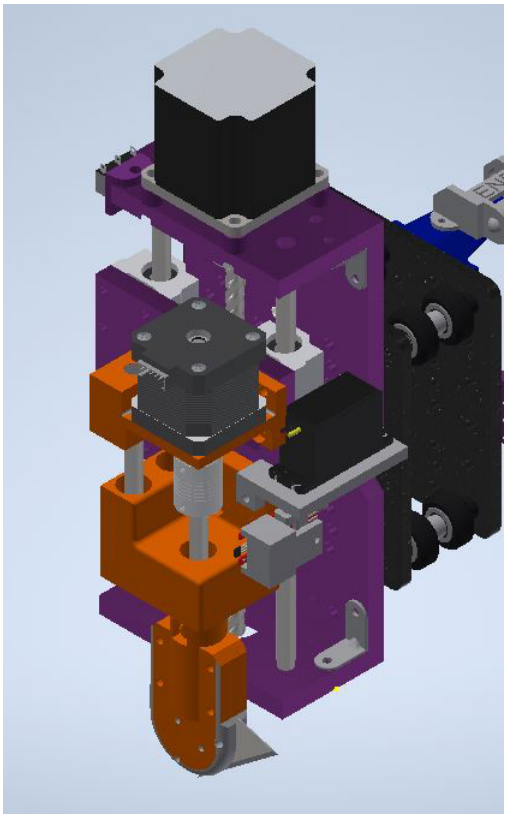

Figure 25. Z-axis [Designed in Inventor]

The selected screw is a T8 2 mm lead rod with a sliding nut made from brass, Fig. 26, which diameter is 8 mm and the pitch is 2 mm. Due to the fact of the use of a flexible coupling between the motor connection and the rod, there is no collar friction in the diameter. The friction between the brass nut and the bar is 0.44 according to the

coefficient in Table 4:

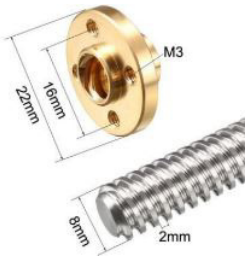

Figure 26. T8 2mm lead rod

Table 4. Brass properties

Materials and Material Combinations		Surface Conditions	Frictional Coefficient	
			Static - μ_{static} -	Kinetic (sliding) - $\mu_{sliding}$ -
Aluminum	Aluminum	Clean and Dry	1.05 - 1.35	1.4
Aluminum	Aluminum	Lubricated and Greasy	0.3	
Aluminum-bronze	Steel	Clean and Dry	0.45	
Aluminum	Mild Steel	Clean and Dry	0.61	0.47
Aluminum	Snow	Wet 0°C	0.4	
Aluminum	Snow	Dry 0°C	0.35	
Brake material[2)]	Cast iron	Clean and Dry	0.4	
Brake material[2)]	Cast iron (wet)	Clean and Dry	0.2	
Brass	Steel	Clean and Dry	0.51	0.44
Brass	Steel	Lubricated and Greasy	0.19	
Brass	Steel	Castor oil	0.11	

Source: Friction Coefficient List from The engineering Toolbox [17]

In order to determine the necessary lifting and lowering torque, the following equation 18 and 17 were used [18]:

$$Tr = \frac{F * dm}{2} * (\frac{\pi * f * dm + l}{\pi * dm - f * l}) + \frac{F * fc * dc}{2} \tag{17}$$

$$Tl = \frac{F * dm}{2} * (\frac{\pi * f * dm - l}{\pi * dm + f * l}) + \frac{F * fc * dc}{2} \tag{18}$$

where:

- Screw diameter: D = 8 mm
- Screw pitch: p = 2 mm

- Frictional coefficient between nut and bar: f = 0.44
- Collar friction: fc = 0
- Frictional diameter of the collar: dc = 0
- Total mass of A and Z axis: 0.906 kg

$$dm = D - \frac{p}{2} \tag{19}$$

$$l = n * p \tag{20}$$

By sustituing equation the variables and equation 19 and 20, the next equation is obtained:

$$Tr = \frac{0.906\ Kg * 9.81\ \frac{m}{s^2} * 7mm}{2} * \frac{\pi * 0.44 * 7\ mm + 4\ mm}{\pi * 7\ mm - 0.44 * 4\ mm} = 0.021\ N * m \tag{21}$$

$$Tl = \frac{0.906\ Kg * 9.81\ \frac{m}{s^2} * 7\ mm}{2} * \frac{\pi * 0.44 * 7\ mm - 4\ mm}{\pi * 7\ mm + 0.44 * 4\ mm} = 0.007\ N * m \tag{22}$$

X-Axis

The profile proposed for the X axis is the C-beam 40x80x1000mm 6063 T5, Fig. 27, as will be seen in the following analyzes to verify its functionality with the X-axis carrige.
To calculate the total force for moving the X-axis carriage, only add the forces of the friction coefficients of the carriage bearings, Table 5, plus the friction force produced by the cutting force of the blade on the plate, equation 6. The slidding system of the car is presented in Fig. 28
Then sustituing the equation 5 and 7 on equation 6:

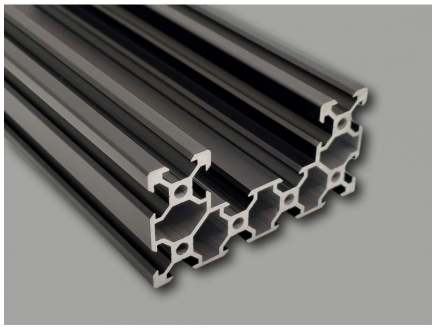

Figure 27. C-beam 40x80x1000 mm 6063 T5 [3]

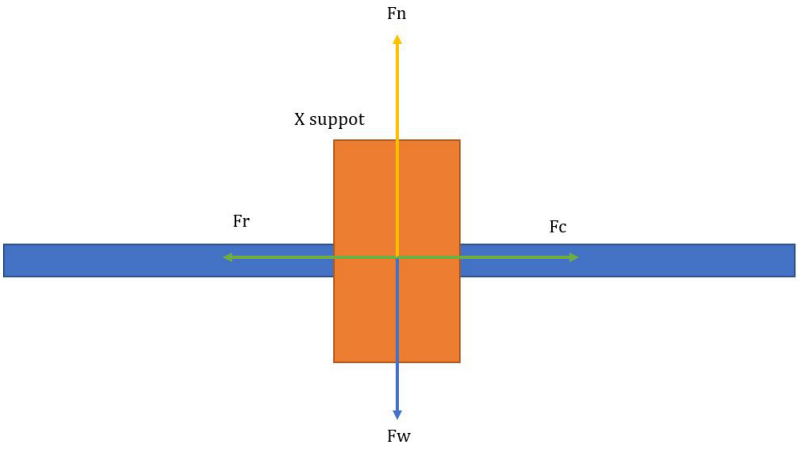

Figure 28. X slidding support car

Table 5. Friction Coefficient on steel bearing

Materials and Material Combinations		Surface Conditions	Frictional Coefficient	
			Static - μ_{static} -	Kinetic (sliding) - $\mu_{sliding}$ -
Aluminum	Aluminum	Clean and Dry	1.05 - 1.35	1.4
Aluminum	Aluminum	Lubricated and Greasy	0.3	
Aluminum-bronze	Steel	Clean and Dry	0.45	
Aluminum	Mild Steel	Clean and Dry	0.61	0.47
Steel	Steel	Clean and Dry	0.5 - 0.8	0.42
Steel	Steel	Lubricated and Greasy	0.16	
Steel	Steel	Castor oil	0.15	0.081
Steel	Steel	Stearic Acid		0.15

Source: Friction Coefficient List from The engineering Toolbox [17]

- Friction coefficient of bearing: u_b = 0.08
- Mass of the x carriage: m = 0.906 kg

$$Fn = Fw = m * g = 0.906\ Kg * 9.81\ \frac{m}{s^2} = 8.887\ N \tag{23}$$

$$Frt_x = u*(Fn+Fs)+u_b*Fn_x = 3*(6.199\ N+0.72\ N)+0.08*(8.887\ N) = 21.43\ N \tag{24}$$

Resulting in a total force to overcome of 21.43 N to provide the movement in the x- axis direction.

Calculation of the X-axis gantry structure

For the calculations of the X-axis structure, the beam to be used is chosen to be a C-Beam aluminum extrusion 40x80x100mm. For load analysis, the dead weight of the beam itself and the total weight of the carriage of the X axis that leads to the Z axis and A axis are considered, the first as a distributed load and the second one as a point load in the most critical region that is in the center of the beam.

- Beam Weight = 1.5 kg [19]
- X carriage Weight = 0.906 kg

Then:

$$Point\ Load = 0.906kg * 9.81\frac{m}{s^2} = 8.887\ N \tag{25}$$

$$Distributed\ Load = \frac{1.5kg}{m} * 9.81\frac{m}{s^2} = 14.715\ \frac{N}{m} \tag{26}$$

It is proceed to perform the calculations of shear forces and moments based on Fig. 28 with two supports, one simple and one articulated Fig 29. So the Fig. 30 and 31 represent these forces and moments.

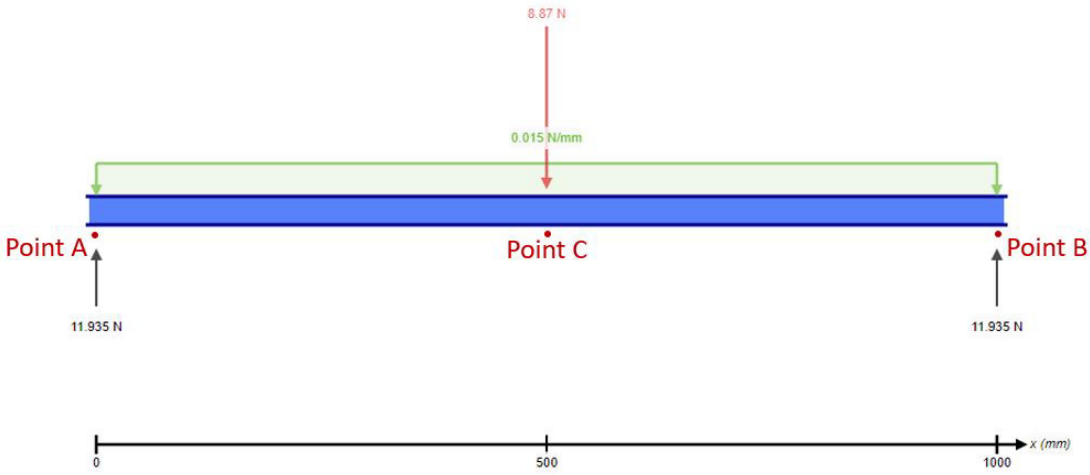

Figure 29. Load Analysis [Made in Skyciv]

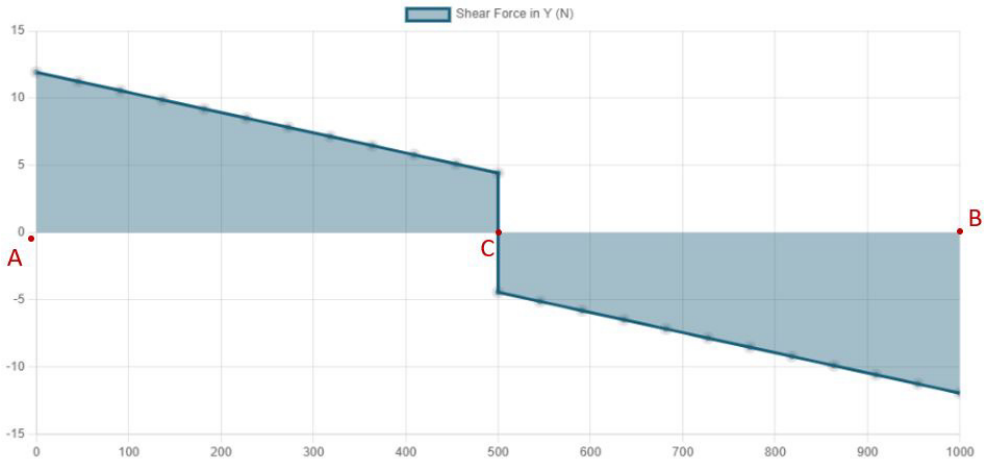

Figure 30. Shear Force Diagram of X beam [Made in Skyciv]

As a result, it is calculated:

$$Reaction : R_0 = 11.935\ N \tag{27}$$

$$Reaction : R_{1000} = 11.935\ N \tag{28}$$

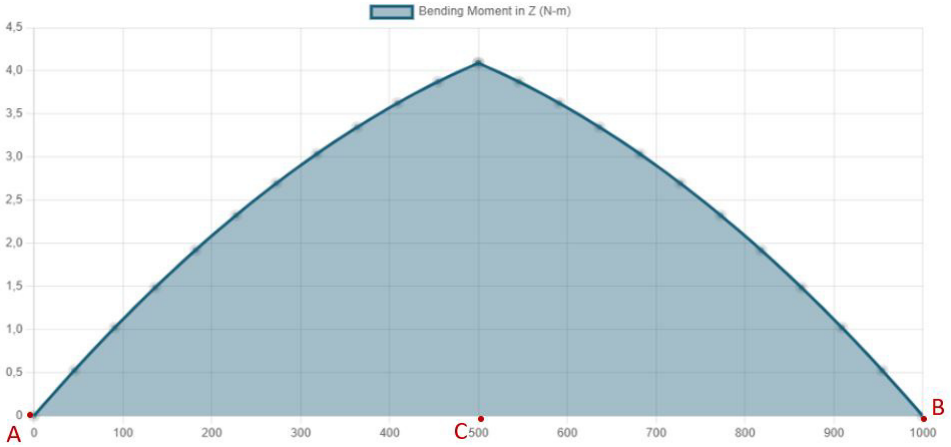

Figure 31. Bending Moment Diagram of X beam [Made in Skyciv]

$$Shear\ Force : V_{max} = 11.935\ N \tag{29}$$

$$Max\ Bending : M_{max} = 4.093\ N.m \tag{30}$$

Fatigue Life of X beam

Once the maximum shear force and its maximum moment have been calculated, a fatigue life relationship can be established with the equations 31 [4]:

$$Number\ of\ cyles : N = (\frac{Se}{a})^{1/b} \tag{31}$$

$$a = \frac{(f * S_{ut})^2}{Se} \tag{32}$$

$$b = \frac{-1}{3} * log(\frac{f * S_{ut}}{Se}) \tag{33}$$

where:

- Se = Endurace limit strength
- Sut = Ultimate strength
- f = fatigue strength fraction

Then it is necessary to establish fatigue limit factors according to the properties of the aluminium 6063 T5 of the beam [16], which correspond to the following development:

- Sut = 186 Mpa
- Sy = 145 MPa
- **Surface Factor ka**: The surface of test specimens is usually highly polished, whereas actual parts usually have rough surfaces. In this case the machined type is choosen, Fig 6.

Table 6. Surface Factor ka

Surface Finish	Factor a S_{ut}, kpsi	Factor a S_{ut}, MPa	Exponent b
Ground	1.34	1.58	−0.085
Machined or cold-drawn	2.70	4.51	−0.265
Hot-rolled	14.4	57.7	−0.718
As-forged	39.9	272.	−0.995

Source: Fatigue failure of beams [4]

$$ka = a(S_{ut})^b = 4.51 * (186\ MPa)^{-0.265} = 1.129 \tag{34}$$

- **Size Factor kb**: size modification during life cycle, Fig

$$de = 0.808 * \sqrt{h * b} = 0.808 * \sqrt{40\ mm * 80\ mm} = 45.707\ mm \tag{35}$$

$$k_b = \begin{cases} (d/0.3)^{-0.107} = 0.879d^{-0.107} & 0.11 \leq d \leq 2 \text{ in} \\ 0.91d^{-0.157} & 2 < d \leq 10 \text{ in} \\ (d/7.62)^{-0.107} = 1.24d^{-0.107} & 2.79 \leq d \leq 51 \text{ mm} \\ 1.51d^{-0.157} & 51 < d \leq 254 \text{ mm} \end{cases}$$

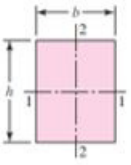

$$A_{0.95\sigma} = 0.05hb$$
$$d_e = 0.808\sqrt{hb}$$

Figure 32. Size Factor kb [4]

$$kb = 1.24 * (de)^{-0.107} = 1.24 * (45.707)^{-0.107} = 0.824 \tag{36}$$

- **Loading Factor kc**: loading modification during life cycle, Fig 33.

$$k_c = \begin{cases} 1 & \text{bending} \\ 0.85 & \text{axial} \\ 0.59 & \text{torsion}^{17} \end{cases}$$

Figure 33. Loading Factor kc [4]

$$kc = 1 \tag{37}$$

- **Temperature Factor kd**: this factor is considered as the ambient operating temperature of the structure, Fig 7

  Being its factor equal to S_T/S_{rt}, where S_T is the resistance to stress at operating temperature and S_{RT} the tensile strength at room temperature, then its choosen value, considering a normal operation, is:

Table 7. Temperature Factor kd

Temperature, °C	S_T/S_{RT}	Temperature, °F	S_T/S_{RT}
20	1.000	70	1.000
50	1.010	100	1.008
100	1.020	200	1.020
150	1.025	300	1.024
200	1.020	400	1.018
250	1.000	500	0.995
300	0.975	600	0.963
350	0.943	700	0.927
400	0.900	800	0.872
450	0.843	900	0.797
500	0.768	1000	0.698
550	0.672	1100	0.567
600	0.549		

Source: Fatigue failure of beams [4]

$$kd = 1 \tag{38}$$

- **Reliability Factor ke**: the assigned reliability factor is 99 percent for its fatigue estimate, Fig 8 then:

Table 8. Reliability Factor ke

Reliability, %	Transformation Variate z_a	Reliability Factor k_e
50	0	1.000
90	1.288	0.897
95	1.645	0.868
99	2.326	0.814
99.9	3.091	0.753
99.99	3.719	0.702
99.999	4.265	0.659
99.9999	4.753	0.620

Source: Fatigue failure of beams [4]

$$ke = 0.814 \tag{39}$$

- **Miscellaneous Factor kf**: This factor aims to achive unspected reduction in endurance limit due to all other effects as residual stress, erosion, etc, Fig 40.

$$kf = 1 \tag{40}$$

- **Se'**: It is test specimen estimated endurace limit.

  In this case as $S_{ut} < 70\ kpsi(482.63MPa)$, then f is equal to 0.9, acoording to the Fig. 34.

$$S'_e = \begin{cases} 0.5S_{ut} & S_{ut} \leq 200 \text{ kpsi (1400 MPa)} \\ 100 \text{ kpsi} & S_{ut} > 200 \text{ kpsi} \\ 700 \text{ MPa} & S_{ut} > 1400 \text{ MPa} \end{cases}$$

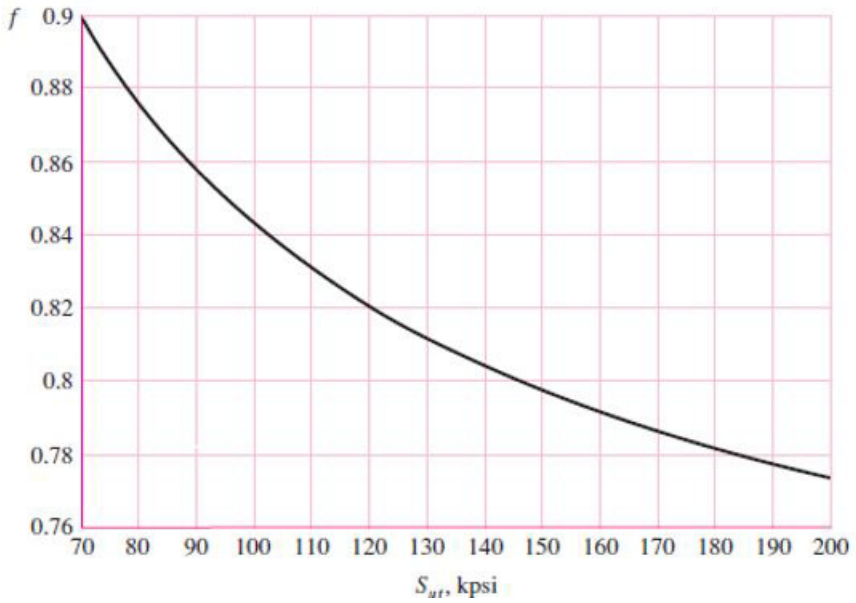

Figure 34. Endurance limit and fatigue strength [4]

$$Se' = 0.5 * S_{ut} = 0.5 * 186MPa = 93\ MPa \tag{41}$$

The next step is calculate the endurance limit Se by introducing the already calculated factors, as:

$$Se = ka * kb * kc * kd * kekf * Se' = 70.415\ MPa \tag{42}$$

Then this coefficients are replaced in equations 32, 33 and 31. Resulting in equation 44.

$$N = \left(\frac{Se}{\frac{(f*Sut)^2}{Se}}\right)^{1/(\frac{-1}{3}*log(\frac{f*Sut}{Se}))} \tag{43}$$

$$N = \left(\frac{70.415\ MPa}{\frac{(0.9*186\ MPa)^2}{70.415\ MPa}}\right)^{1/(\frac{-1}{3}*log(\frac{0.9*186\ MPa}{70.415\ MPa}))} = 1000000\ [Cycles] \tag{44}$$

In this way, a number of useful life cycles of 10e6 is obtained until reaching the endurance limit of the material, where it is ensured that failure will not occur due to cycle fatigue entering the infinite life region, as in example of Fig. 35.

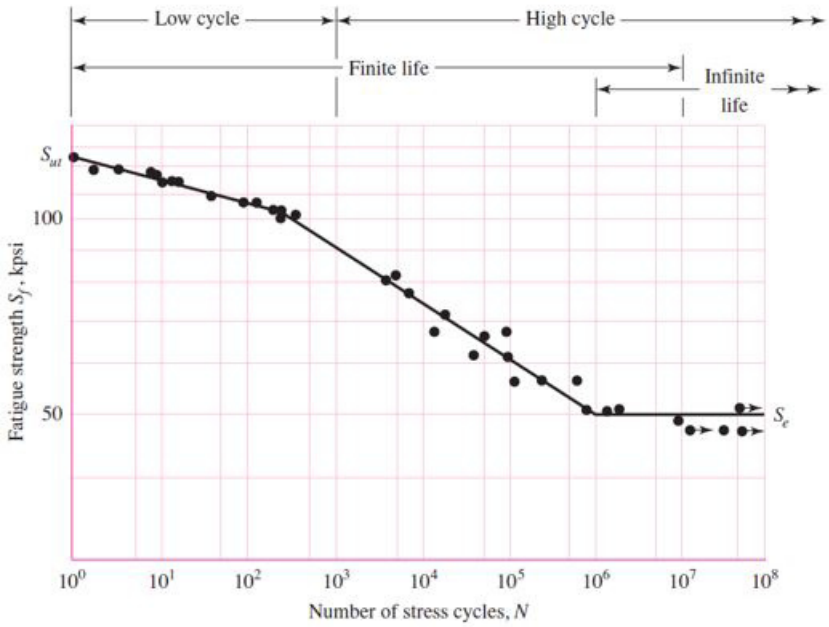

Figure 35. Stress life cycles [4]

Fatigue failure criteria for stress in X-axis

The failure criteria are based on the stresses associated with the mean fluctuating stress and its amplitude or alternating component [4]. In this analysis, the ASME Elliptic criteria will be used to determine the life safety factor with respect to the chosen

material of 6063 aluminum, as in the equation 45.

$$nf = \sqrt{\frac{1}{(\frac{\sigma_a}{Se})^2 + (\frac{\sigma_m}{Sy})^2}} \tag{45}$$

Where:

$$\sigma_a = \frac{\sigma_{max} - \sigma_{min}}{2} \tag{46}$$

In this case by using extremely low load values, $\sigma_{min} = 0$ and $\sigma_a = \sigma_m$.

σ_{max} is calculated by means of equation .

$$\sigma_{max} = \frac{M_{max} * y}{I} \tag{47}$$

Dimensions of the C-beam [3]:

- Length: b = 40 mm
- Height: h = 80 mm
- Second moment of Inertia Y-axis: I = 112.278*10^{-9} m^4

$$y = \frac{h}{2} = \frac{80mm}{2} = 40\ mm \tag{48}$$

By replacing the equations 48, 47 in equation 49.

$$\sigma_a = 0.695\ MPa = \sigma_m \tag{49}$$

And finally calculating the factor of safety by replacing the values of Se, σ_a, σ_m and Sy, the value is expressed in equation 50.

$$nf = 91.13 \tag{50}$$

In the Fig. 36 the proposed design can be seen allowing the movility with a 8 mm pitch power screw connected to a flexible coupling and a safety factor of the C-beam of 91,13. This was chosen by the market´s component standards of the region, since it was the simplest mechanism to acquire in the market.

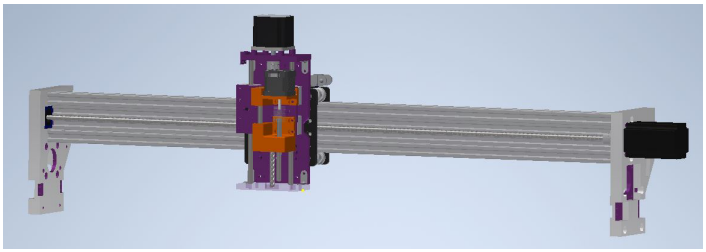

Figure 36. Proposed X axis design [Made in Inventor]

The deflection of the C-beam is calculated with the equation 51 [20] using the properties of the material 6063 T5 [3] with the forces acting on the beam.

- Length of the beam: L = 1 m
- Modulus of Elasticity: E = 68.99*10^9 N/mm^2
- Point/distributed force: P_i

$$Max\ deflection = \sum(Di_{max}) = \frac{P_i * L^3}{192 * E * Ix} \tag{51}$$

$$D1_{max} = \frac{8.887\ N * 1\ m^3}{192 * 68.99 * 10^9\ \frac{N}{mm^2} * 117.780 * 10^{-}9\ m^4} \tag{52}$$

$$D2_{max} = \frac{14.71\ N * 1\ m^3}{192 * 68.99 * 10^9\ \frac{N}{mm^2} * 117.780 * 10^{-}9\ m^4} \tag{53}$$

$$Max\ deflection = D1_{max} + D2_{max} = 0.01161\ mm \tag{54}$$

Table 9 shows the values of the maximum allowable deflection depending on which part of the machine needs to be calculated according to the desired precision following the equation 55.

Table 9. Maximum allowable deflection

Maximum bending at the length of the beam	Precision
0.003 mm/mm-L	General part of a machine
0.0005 mm/mm-L	Moderate precision
0.00001 mm/mm-L	High precision

Source: Material resistance [20]

$$allowable\ deflection = \frac{0.0005\ mm}{mm - L} * L_{beam} = \frac{0.0005\ mm}{mm} * 1000\ mm = 0.5\ mm \tag{55}$$

Comparing the maximum deflection allowed with the theoretical deflection of the C-beam, the safety factor is obtained based on equation 56. It must be taken into account that the calculation made is for a beam with alternating loads exist due to the operation of the CNC. Therefore, a load factor due to fatigue equal to 3 is added.

$$n_{deflection} = \frac{allowable\ deflection}{3 * Max\ deflection} = \frac{0.5\ mm}{3 * 0.01131\ mm} = 14.73 \tag{56}$$

The safety factor obtained from the calculation for rigidity, of 14.73, ensures that the beam does not exceed the maximum deflection allowed. In addition, to verify the cal-

culations of the design by rigidity, the axis was simulated in the Autodesk Inventor Professional, using finite elements, the results obtained from the simulation can be observed in Fig. 37.

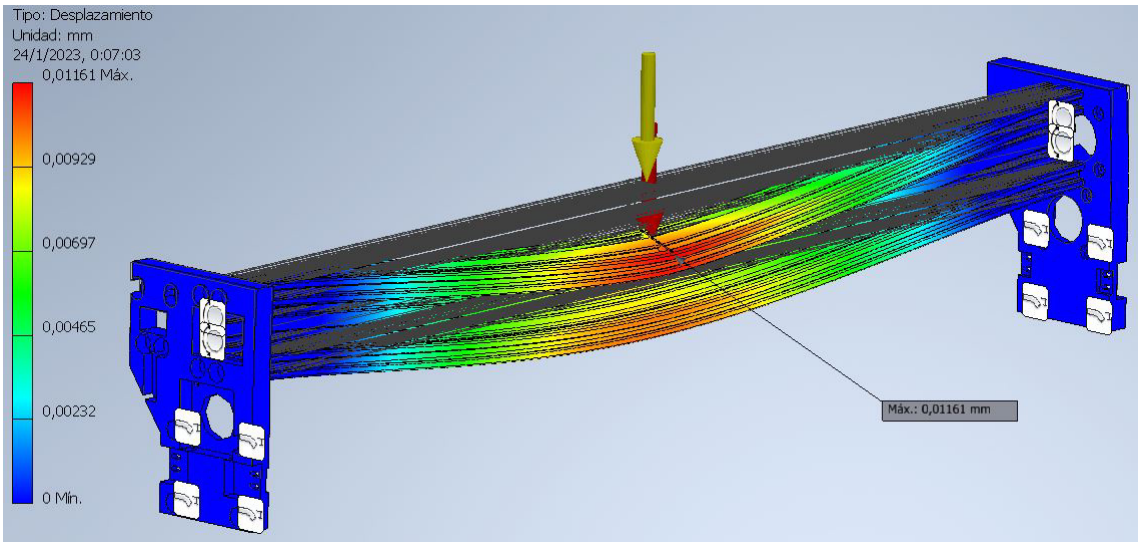

Figure 37. FEA Simulation: Stress and deformation analysis in X axis, view x1 [Made in Inventor]

In the simulation, Fig 37, a maximum deflection value equal to 0.01161 mm is obtained, which verifies the value obtained by the theoretical calculation.

3.5. Y-Axis Mechanism

The proposed design for the Y-axis mechanism is shown in Fig. 38. This design implements a direct transmission of the motor force to the axis where it moves, this is thanks to the use of 20-tooth GT2 pulleys in conjunction with a 6 mm wide GT2 belt and a 2 mm pitch. Fig 39, acting on the surface of the V-slot beam 20x40x1000 mm, Fig. 40.

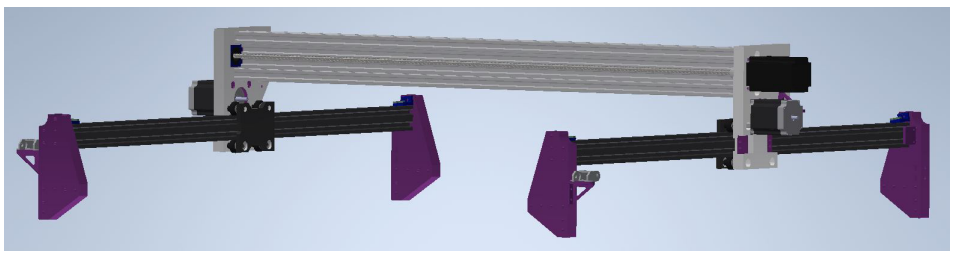

Figure 38. Proposed Y axis design [Made in Inventor]

Figure 39. GT2 Pulley and Belt 6 mm

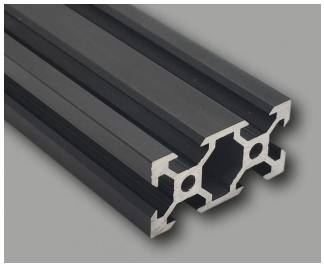

Figure 40. V-slot beam 20x40x1000 mm [5]

The approximate mass is calculated from the inventor's software, giving a value of 2.5 kg. Its force applied on one shaft is given by the equation 57.

$$Fw = m * g = 2.5kg * 9.81\frac{m}{s^2} = 24.52\ N \tag{57}$$

To obtain the total force the y axis must generate, the drag force generated by this system is added plus the necessary cutting force.

$$Fw = Fn \tag{58}$$

The friction coeficient is taken by the Table 4.

$$Fr = u * Fn = 0.08 * 24.52N = 1.96\ N \tag{59}$$

$$Frt_y = Fr + Fr_{blade} = 1.96N + 20.76N = 22.72\ N \tag{60}$$

Therefore, the necessary cutting force for this axis to overcome is 22.72 N

Calculation of the Y-axis gantry structure

The calculation of the Y- structures is based on the use of a 20x40x1000 mm V slot aluminium extrusion made from aluminium 6063 [5]. The procedure of the load analysis is the same as in the section of X mechanism. Two weight are considered, the first is the weight of the beam as distributed load, and the second one is the weight of the Z and X mechanism which is sliding on the Y beam, this load is located in the center as the critical region to analyze as in Fig. 28.
The total weight of the carriage is structured by the weight of the X motor, a Y motor, the average weight of the coupling parts of the Y axis and the entire set of the Z axis with the A axis, this because it is intended to put in the conditions most extreme loads that can occur on one of the Y axes.

- Beam Weight = 0.937 kg [21]
- Total Carriage Weight = 3.636 kg

Then:

$$Point\ Load = 3.636kg * 9.81\frac{m}{s^2} = 35.66\ N \tag{61}$$

$$Distributed\ Load = \frac{0.937\ kg}{m} * 9.81\ \frac{m}{s^2} = 9.19\ \frac{N}{m} \tag{62}$$

In Fig.41 the load analysis is shown with its force and moment diagrams.
As a result, it is calculated:

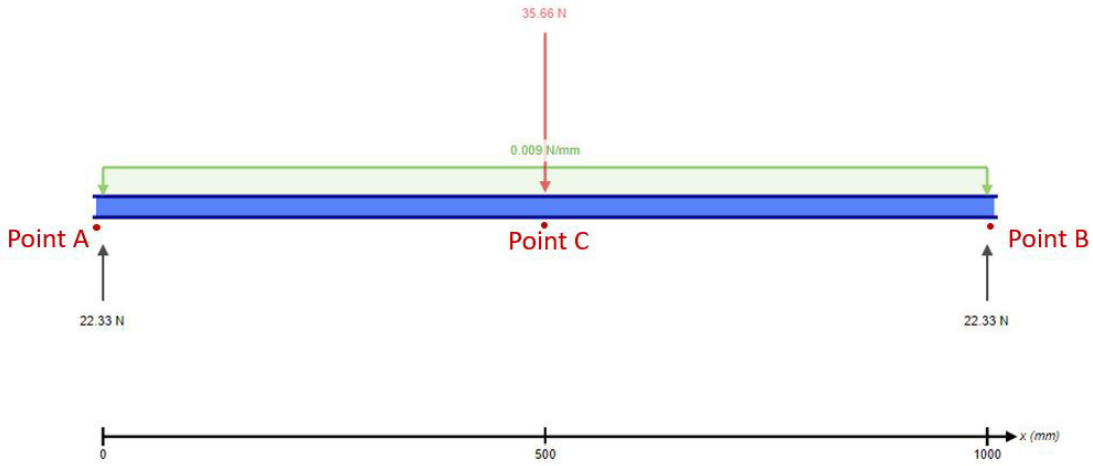

Figure 41. Load Analysis [Made in Skyciv]

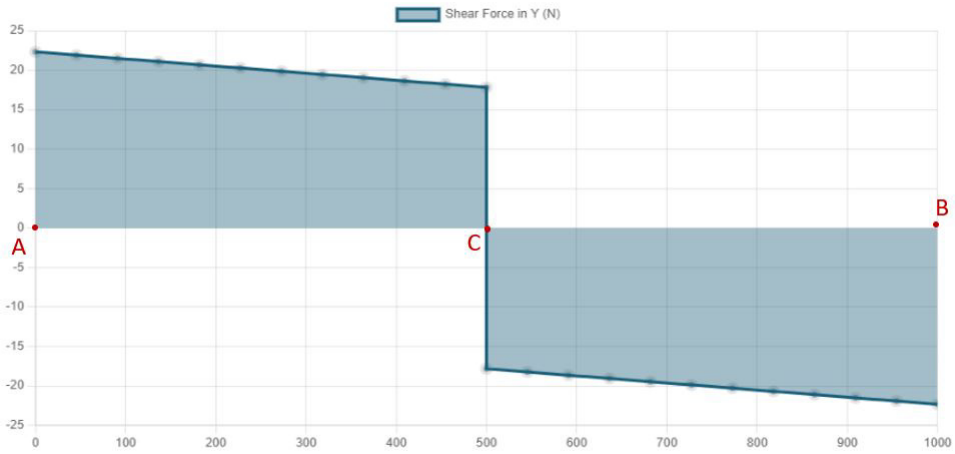

Figure 42. Shear Force Diagram of X beam [Made in Skyciv]

$$Reaction : R_0 = 22.33\ N \tag{63}$$

$$Reaction : R_{1000} = 22.33\ N \tag{64}$$

$$Shear\ Force : V_{max} = 22.33\ N \tag{65}$$

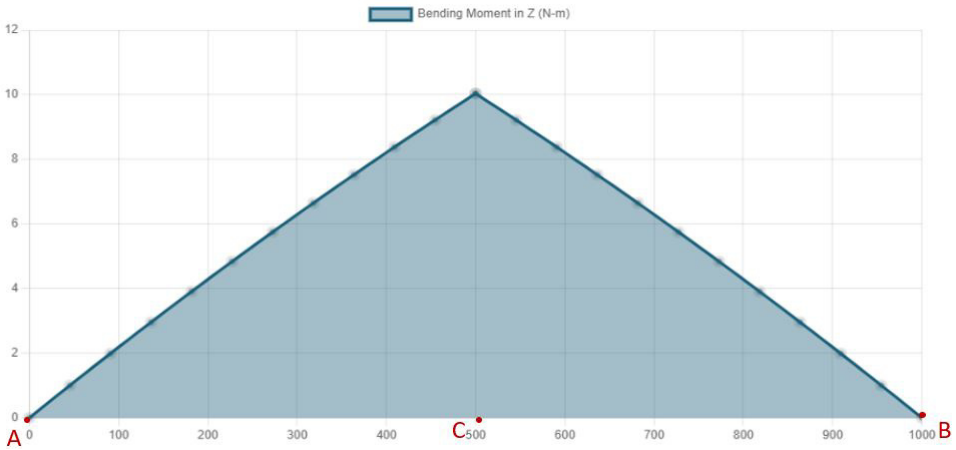

Figure 43. Bending Moment Diagram of Y beam [Made in Skyciv]

$$Max\ Bending : M_{max} = 10.04\ N.m \tag{66}$$

Fatigue Life of Y beam

With the same equations of the section ”Fatigue life of X beam” (equations 32, 33, 42), but taking the new values of of the beam, the result are presented as follows:

- a = 369.518
- b = -0.115
- Se = 75.83 MPa

$$Number\ of\ cyles : N = (\frac{Se}{a})^{1/b} = (\frac{75.83}{369.518})^{1/-0.105} = 1 * 10^6\ [cycles] \tag{67}$$

Proving by the equation 67, according to the example in Fig. 35 that the profile is also in an infinite life cycle after iteration number of $1 * 10^6$.

Fatigue failure criteria for stress in Y-axis

Likewise, the ASME Elliptic criterion was used to determine the safety factor of the profile. By replacing the new values in equations 45, 47, 48 and 49. σ_{max} and taking

$\sigma_a = \sigma_m$. The results are shown in equations 68 and 70.

- Width of the beam: b = 20 mm
- Height of the beam: h = 40 mm
- Second moment of Inertia X-axis: I = 48.163*10^9 m^4

$$\sigma_{max} = \frac{M_{max} * y}{I} = \frac{10.04\ N.m * 30\ mm}{48.163 * 10^9\ m^4} = 4.169\ MPa \tag{68}$$

$$\sigma_a = \frac{\sigma_{max} - \sigma_{max}}{2} = 2.0845\ MPa \tag{69}$$

$$nf = \sqrt{\frac{1}{(\frac{\sigma_a}{Se})^2 + (\frac{\sigma_m}{Sy})^2}} = \sqrt{\frac{1}{(\frac{2.0845\ MPa}{75.83\ MPa})^2 + (\frac{2.0845\ MPa}{145\ MPa})^2}} = 32.23 \tag{70}$$

The deflection of the V slot is calculated with the equation 71 [20] using the properties of the material 6063 T5 [16] with the forces acting on the beam.

- Length of the beam: L = 1 m
- Modulus of Elasticity: E = 68.99*10^9 N/mm^2
- Point/distributed force: P_i

$$Max\ deflection = \sum(Di_{max}) = \frac{P_i * L^3}{192 * E * Ix} \tag{71}$$

$$D1_{max} = \frac{35.66\ N * 1\ m^3}{192 * 68.99 * 10^9\ \frac{N}{mm^2} * 48.163 * 10^{-}9\ m^4} \tag{72}$$

$$D2_{max} = \frac{9.19\ N * 1\ m^3}{192 * 68.99 * 10^9\ \frac{N}{mm^2} * 48.163 * 10^{-}9\ m^4} \tag{73}$$

$$Max\ deflection = D1_{max} + D2_{max} = 0.071\ mm \tag{74}$$

Using the same Table 9 as in section of X mechanism, the maximum allowable deflection on the beam is calculated, equation 75.

$$allowable\ deflection = \frac{0.0005\ mm}{mm - L} * L_{beam} = \frac{0.0005\ mm}{mm} * 1000\ mm = 0.5\ mm \tag{75}$$

As previous explained on section of X mechanism, the safety factor for the v slot beam is calculated with the equation 76, and as well it must be added a fatigue factor equal 3 due to the conditions of the alternating loads acting on the beam.

$$n_{deflection} = \frac{allowable\ deflection}{3 * Max\ deflection} = \frac{0.5\ mm}{3 * 0.071\ mm} = 2.347 \tag{76}$$

As result, a safety factor of 2.347 is calculated for the v slot beam to ensure it does not exceed the maximum deflection allowed. In addition its deflection is simulated in Autodesk Inventor, Fig. 44.

In the simulation, Fig 37, a maximum deflection value equal to 0.07358 mm is calculated, which verifies the value obtained by the theoretical calculation.

3.6. Trajectory X and Y components

Once the total forces of each component X and Y have been obtained, equation 24 and 60, the total required force can be obtained when the trajectory has these components in equation 77 and can be represented in Fig. 45.

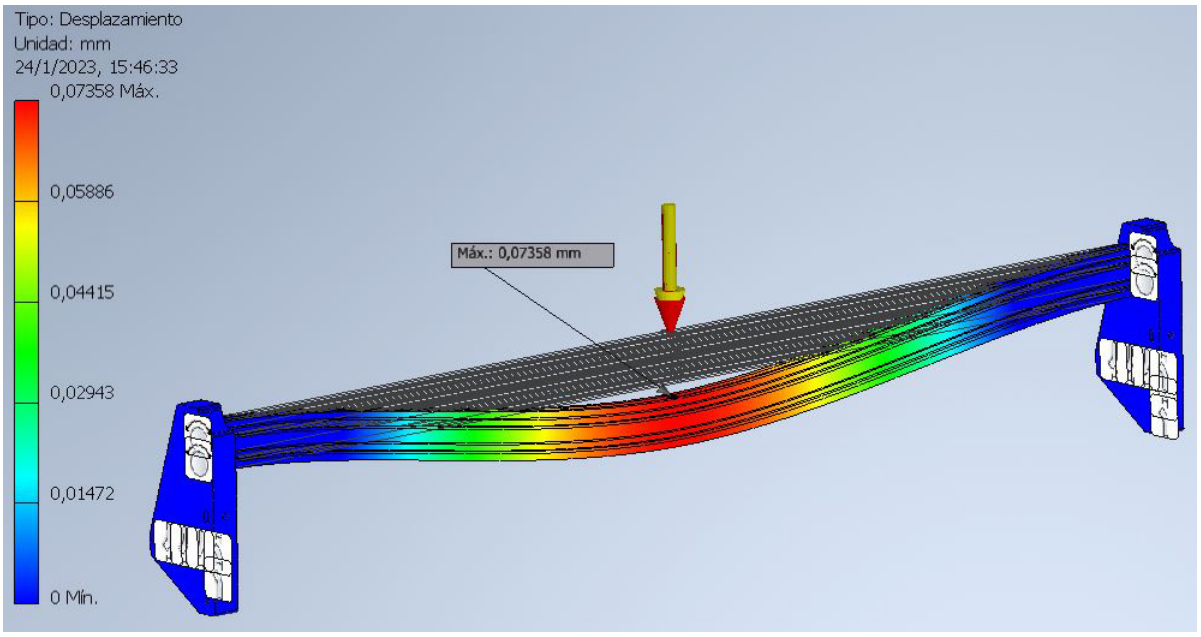

Figure 44. FEA Simulation: Stress and deformation analysis in Y axis, view x1 [Made in Inventor]

$$F_{xy} = \sqrt{(Fx)^2 + (Fy)^2} = \sqrt{(21.43\ N)^2 + (22.72\ N)^2} = 31.23\ N \tag{77}$$

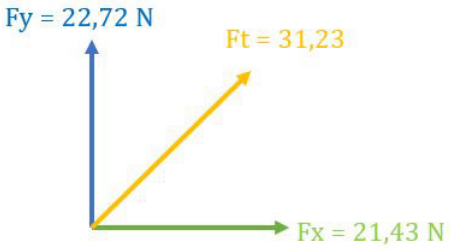

Figure 45. Total required force applied in the X and Y coordinates

3.7. Motor Selection

A-axis Motor

Since the tangential blade is dragged by the trajectory positions of the X and Y axis, the resistance rotation force that the motor must overcome is almost zero, so it is neglected, its drag movement is observed in Fig. 46.

The reason for what is required the A-axis instead, of necglect this axis and just located

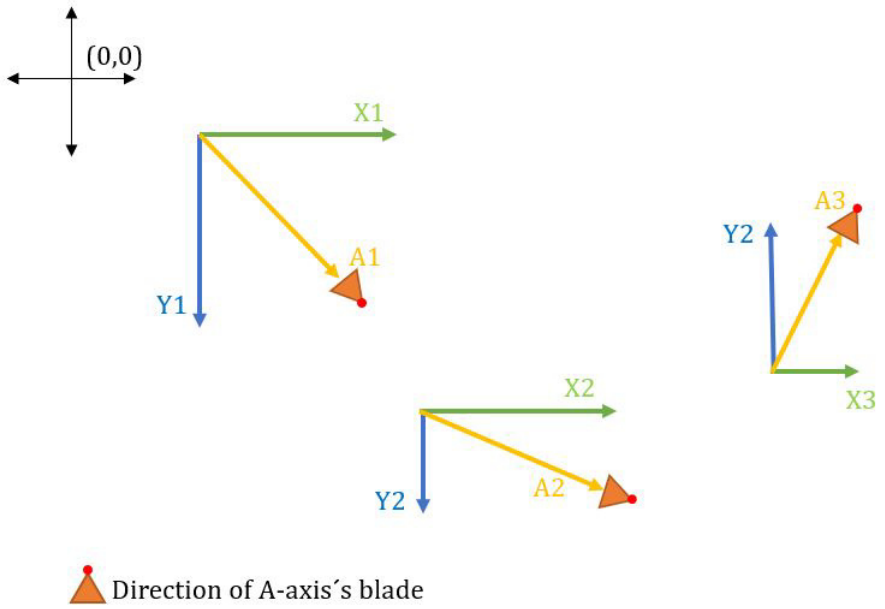

Figure 46. A-axis dragged example

a dragged shaft with a blade, it´s because of 3 reasons, the first one is the need of a zero position for the fourth axis, which is difficult to achieve manually, the second reason is due to the control of the fourth axis, the cutting time of a product can be reduced, because, while the blade is being transferred to another point of the material in the clear area, the blade can be relocated automatically so that when it start at the other point, the blade is already in the correct position, and the third and last reason is that the cutting of a sheet with a thickness of more than 1 mm is more efficient [22], due to the control maneuverability offered by the last axis. The only force it must hold is the perpendicular force created when cutting the material given in the equation 1 when the blade is alligned to the trajectory of X and Y axis.

For this reason, a low-torque Nema 17 motor is selected within the price-quality range is more than enough. Fig 47.

- Torque = 15 N.cm
- Voltage = 12V
- Current = 1.2 A
- Step per revolution = 200

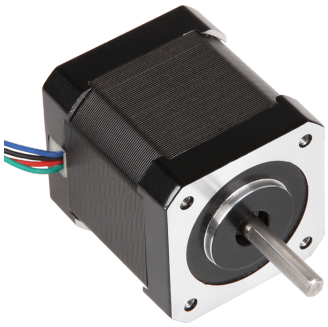

Figure 47. Nema 17 [6]

Z-axis Motor

Nema17 motors have a torque of 15 N.cm, and the maximum torque value obtained in the equation 22 is 21 N.cm, a low-torque Nema23 motor from this range is selected, as seen in Fig. 48 which has the following characteristics:

- Voltage = 24 V
- Current = 2.5 A
- Torque = 80 N.cm
- Step angle = 1.8°
- Step per revolution = 200

Figure 48. Nema 23 M1233022 [7]

Thus considering a safety factor in the equation 78:

$$ns = \frac{80\ N.cm}{21\ N.cm} = 3.81 \tag{78}$$

In this way, the equation 78 shows that the safety factor for the necessary torque is 3.8, resulting in the safe force being 3 times greater than required force.

X and Y axis Motor

According to the equations 24 and 60 the force to overcome in X-axis is about 21.43 N and 22.72 N in y-axis, it can be established again that the price-quality motor that satisfies the requirements is a Nema 23 motor with the same features of the Z axis, Fig.**??**, and a safety factor as follows:

$$ns_x = \frac{72\ N.cm}{21.43\ N.cm} = 3.35 \tag{79}$$

$$ns_y = \frac{72\ N.cm}{22.72\ N.cm} = 3.16 \tag{80}$$

3.8. Axis's Steps Configuration

In a step motor, the motor's rotor moves in discrete steps, or increments, rather than continuously as in a conventional motor. The size of these steps is determined by the microstep configuration of the motor.

A microstep configuration is a way of subdividing each step of a step motor into smaller increments, allowing for finer resolution and smoother motion. This is achieved by electronically dividing the number of steps per revolution of the motor into a larger number of microsteps. There are a few different microstep configurations that are commonly used, including 1/2, 1/4, 1/8, 1/16, and 1/32 microsteps.

To have a standard precision and equity of not losing torque, the use of a microstep of 1/16 is chosen by default for each motor.

X-axis

The equation for the calculation of microsteps in the X axis is given by the use of a 8 mm pitch screw, [23]:

$$X_r = \frac{Step\ per\ revolution}{pitch * microsteps} = \frac{200\ steps}{8\ mm * \frac{1}{16}} = 400\ \frac{step}{mm} \tag{81}$$

Y-axis

On the other hand, the calculation of the resolution of the motors in the Y axis is given by the equation 82 considering the pulley and belt´s parameter explained in section (Y-axis mechanism).

$$Y_r = \frac{Step\ per\ revolution}{pitch\ belt * Number\ of\ deeth\ on\ the\ pulley * microsteps} = \frac{200\ step}{2\ mm * 20 * \frac{1}{16}} = 80\ \frac{step}{mm} \tag{82}$$

Z-axis

As in the x axis, the equation for the calculation of microsteps in the z axis is given by the use of a 4 mm pitch screw: [23]

$$Z_r = \frac{Step\ per\ revolution}{pitch * microsteps} = \frac{200\ steps}{4\ mm * \frac{1}{16}} = 800\ \frac{step}{mm} \tag{83}$$

A-axis

To calculate the steps in axis A, it should be emphasized that this motor has a direct transmission of movement, that is, it does not depend on a system of pulleys or screws like the previous axes and its motion is a rotational trajectory, therefore the resolution equation is given by:

$$A_r = \frac{Step\ per\ revolution}{360° * microsteps} = \frac{200\ steps}{360° * \frac{1}{16}} = 8.888\ \frac{step}{degree} \tag{84}$$

4. Electrical Design

4.1. Power Comsumption

Dimensioning the power consumption of a system allows to ensure that the system is as power efficient as possible. This can help to reduce energy costs and minimize the environmental impact of the system [24]. It helps to ensure that it operates within the limits of its components, improving system reliability, as shown in the table 10.

Table 10. Power Comsuption

Component	Quantity	Voltage [V]	Current [A]	Total Current [A]
Nema23 HS5628	3	24	2	6
Nema23 573S20	1	24	4	4
Nema17 HS3401	1	12	1,2	1,2
Driver TB6600	3	24	0,5	2,4
Driver TB6566	1	24	0,5	0,5
Driver DRV8825	1	12	0,5	0,5
Arduino Mega	1	9	0,073	0,073
RAMPS 1,4 SHIELD	1	9	0,05	0,05
Regulator 7805	1	12	1	1
Regulator 7812	1	12	1	1
Servo MG996r	1	6	0,9	0,9
			Total:	**17.62**

Based on consumption calculations, it is determined that the ideal supply unit for the system should have a maximum voltage of 24 V, and 20 A, in this way the safety factor for the power comsuption is given by equation 85 as:

$$ns_{energy} = \frac{I_{input}}{I_{output}} = \frac{20A}{17.62A} 1.135 \tag{85}$$

4.2. Energy Distribution and Block Diagram

The distribution of energy and signals is divided into 6 blocks:

- **Circuit power:** this block allows to make the first connection from alternating current to direct current through the 24 V source.
- **Protection and voltage regulation:** The first part of this section establishes the connection to a 20 A protection fuse, to avoid over currents that can damage the components, the second part is the distribution and regulation of voltage according to the requirements of each component: 5, 12 and 24 V.
- **Movements:** This block shows the distribution of the motors for each axis.
- Communication: This block shows the connection bridge between the components and the control software.
- **Artificial Inteligence:** Here the acquisition of images as computer vision is applied by means of an external camera that emits the data to the PC as a processing source for the AI service.
- **Software Control:** In this field, all the necessary commands are processed to carry out the AI cutting and verification process.

4.3. Circuit Distribution

The circuit ensures that electrical energy can be efficiently transmitted and distributed to the various locations where it is needed. This circuit design and distribution can help to minimize energy loss and improve the overall efficiency of the electrical system. It is also important for safety, as the fuse protection helps to prevent overloading of circuits and reduces the risk of electrical fires. As taking into account the electrical components the circuit distribution is also a key factor in determining the overall cost of an electrical system, as it can affect the size and number of components required, as well as the cost of installation and maintenance. The circuit is divide into the following parts:

- Voltage supply 24 V.

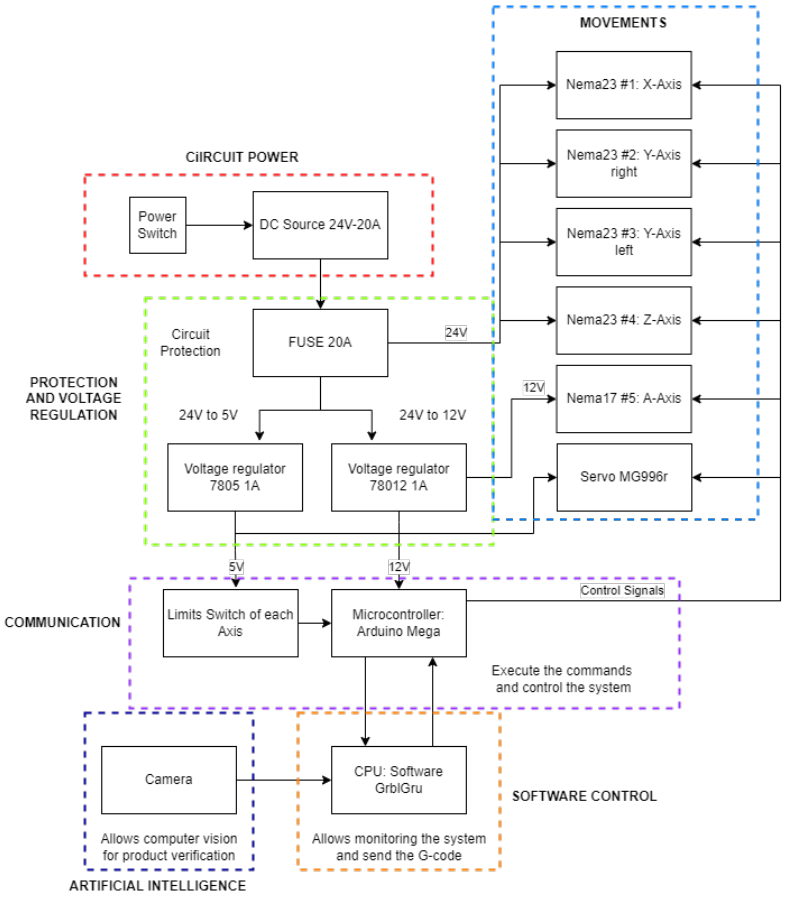

Figure 49. Block Diagram: Power and Signal Distribution [Made in Autocad]

- Voltage regulator 12 V.
- Voltage regulator 5 V.
- Limit switch connections, to filter any unexpected noise in the signal for the homing cycle and distance verification for each axis.
- As weel for the limit switch, the stop signal, which is important to ensure a emergency stop in case of any accident.
- Step drivers connections.

The pcb circuit was made in proteus with the capacity of a two-sided plate with a dimension of 94x79 mm as an optimized average, seen in Fig. 50.

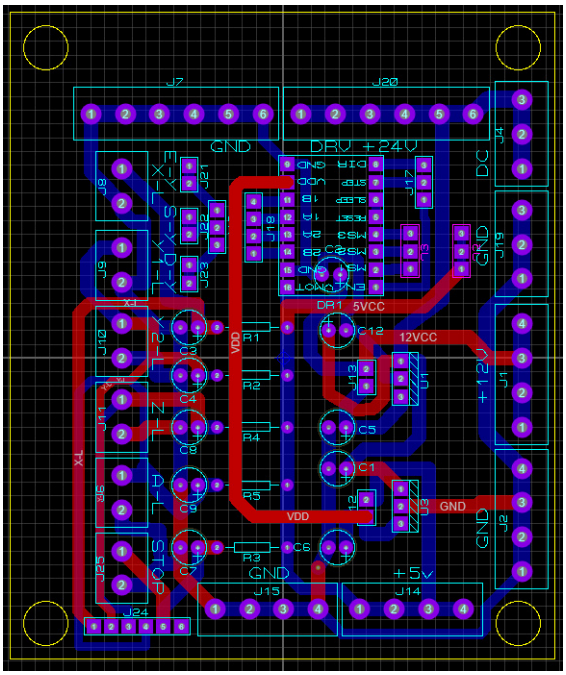

Figure 50. PCB: Control Circuit [Made in Proteus]

4.4. CNC Integration

For the CNC integration an Arduino Mega with a board ramps V1.4 are used. The connections inside ramps 1.4 are made according to the diagram in Fig. 51.

In the Fig. 51, the motor´s connections were made in the X,Y,Z and E0 Section through the pins:

- **EN:** enable the signal to energize the motor.
- **DIR:** direction of the motor.
- **STEP:** the step signal to indicate how far the motor must move.
- **Endstop:** as well the signal of the limit switch where connected in the ”S” pin by knowing a filter circuit is used, so it is no need to do the voltage and ground connections of these pins directly to the board.
- The emergy button and the endstop of the 4th axis is connected in Aux-2.
- Finally, the servo MG996r is connected to the first pins of the servo section. Fig 51.

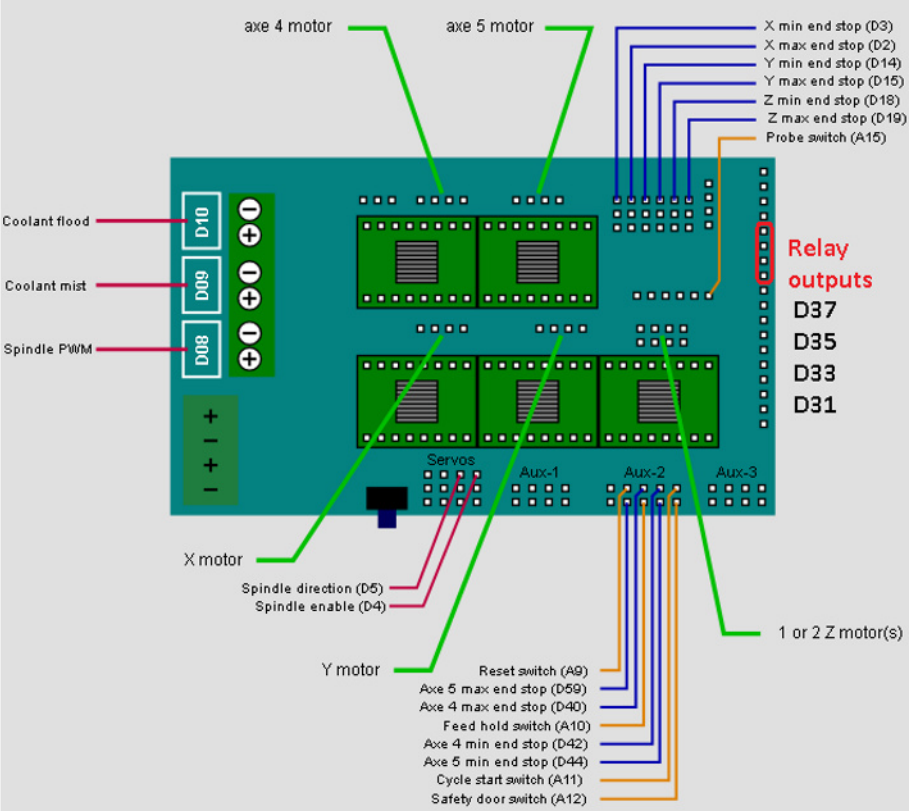

Figure 51. Arduino Mega: Ramps Shield 1.4V [8]

In this way the connections are ready for coupling with the arduino and its operation with the GrblGru software.

5. Computer Design

5.1. Control Firmware: Grbl-Mega-5X

GRBL is open-source firmware that runs on a variety of microcontrollers to control hobby CNC machines such as 3-axis mills and routers. The Mega 5X variant is specifically designed to run on the Arduino Mega 2560, a microcontroller board based on the ATmega2560. It is designed to work with 5-axis machines and provides additional features and capabilities compared to the standard GRBL firmware. [25]

The firmware is downloaded from the main github page ”Grbl-Mega-5X” and flashed on the Arduino Mega microcontroller using the ”Arduino.ino” software. Then the connections are made as shown in Fig. 51.

5.2. Control Software: GrblGru V5.0

GrblGru is a free, open-source 2D G-code generator for Grbl, a CNC controller software. It allows users to create G-code from 2D drawings, such as DXF format, SVG, BMP or import custom g-code. The generated G-code can then be used to control CNC machines as in this case a 4-axis CNC knife. [26]

GrblGru has a user-friendly interface and includes several features to make it easy to use. It allows users to adjust feed rates and tool sizes, and to preview the G-code path before sending it to the CNC machine. It includes support for various shapes and operations, which commomly are difficult to achieve by hand.

5.3. 2D G-code Generator

The 2D G-code generator allows effective monitoring between the user and the configuration of the necessary parameters for the CNC with the ability to preview the G-code path before sending it to the machine. To monitor and analyze the process, the product ”Postre Box” is used with the following dimensions in Fig. 52.

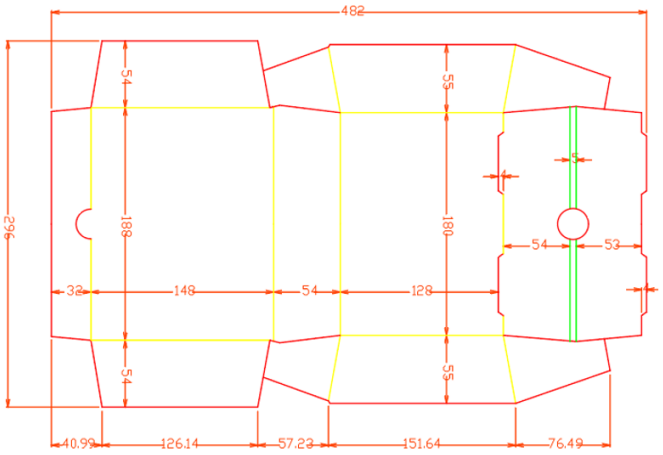

Figure 52. Product: Postre Box [Made in Illustrator]

Once the software is activated, in the 2D section, the following steps to generate the code for the example product ”Postre Box” are:

1. Upload the SVG, DXF or BMP file.
2. Rename the layers according to the two jobs to be performed: profile cut (P), bending cut (R). Fig. 54

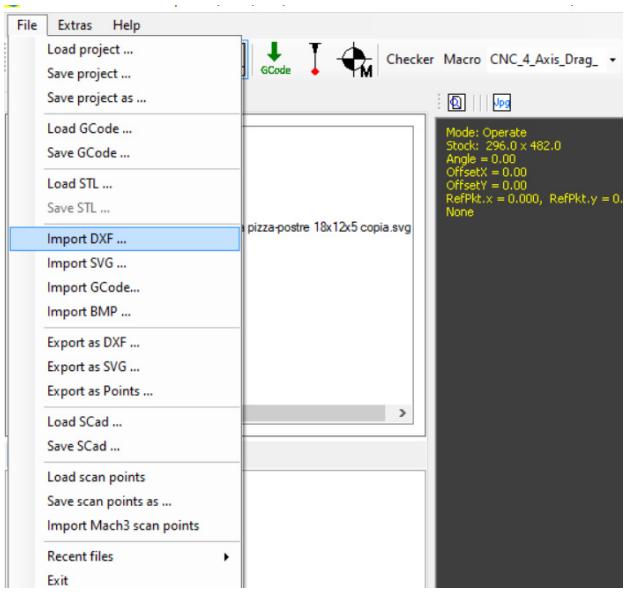

Figure 53. 2D Section: Importing file [From GrblGru]

3. Generate the custom ”Job”, called ”CNC: Cut tangential blade” as in Fig. 55.

   The general configurations of the job is shown in Fig. 56. The main parameter according to the settings of th CNC are:

   - ”Depth Increment” and ”Sum of increments”: as the job is planned to be just one cut, is normal to set it as just one turn of 3 mm depth, Fig. 56.
   - ”Plunge feedrate” and ”Cut feed rate”: it is the speed to use when the tip is plunged into the material and start to cut, Fig. 56.
   - ”Rapid feedrate”: is the speed use when the tip is the clearence zone, which is not in contact with the material, Fig. 56.
   - ”Height of the clearence plane”: is the height set where the rapid feed rate is activated, Fig. 56
   - ”Rotation feedrate”: the 4-axis´s speed, Fig. 56.

5.4. Optimization and post-processing of G-code

For each Job, the G-code generated by GrblGru establishes a path start relationship with an initial speed for the fourth axis of F1000 [mm/min] by default, this consequently determines the first step of each path as ”F1000 A0” Although this does not influence the cutting efficiency, it does determine an extension of unnecessary time for the work,

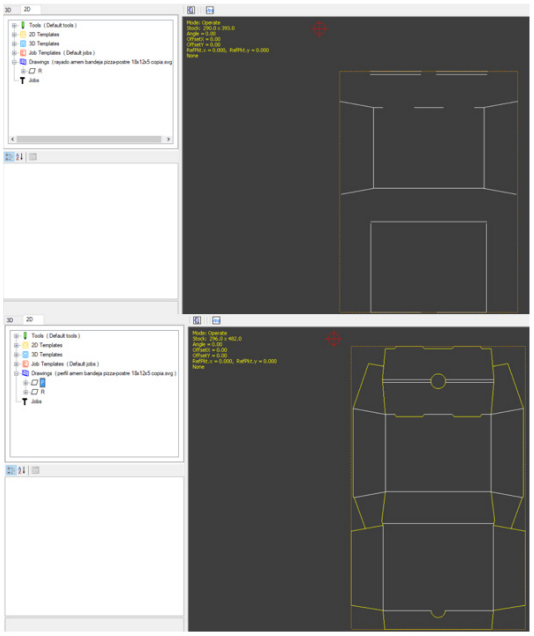

Figure 54. 2D Section: Files [From GrblGru]

considering this code as ”extra” that only consumes time since its function is to make the 4-axis to go zero every time the Z axis is raised for each path as is seen in Fig. 57. The post processing of the generated code is only based on eliminating the extra excess code of each path to reduce the cutting time at the CNC, Fig. 58.
Thanks to this small modification, the cutting time of the product ”Postre Box” was reduced from 22 minutes to 12 minutes, as seen in Fig. 59.

5.5. 3D Control Panel

The control panel of GrblGru is a graphical user interface (GUI) that allows users to control and configure the software. It includes a variety of buttons, menus, and input fields that can be used to perform various tasks and adjust various settings. [27]
Here is a general overview of the different elements that may be included in the GrblGru control panel(Fig. 60):

- **File menu:** This menu allows users to open, save, and import files, as well as access the software’s preferences and other settings, Fig. 60.
- **Drawing area:** This is the main area of the control panel where users can view and edit their 2D drawings. It may also include a preview of the G-code path that

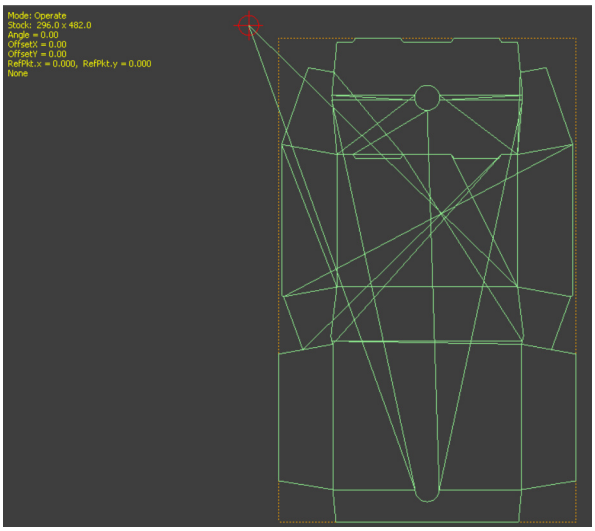

Figure 55. 2D Section: Path [From GrblGru]

1. General	
Main Mode	CUT
Transformation Mode	NONE
2. Type of Tool	
Type of Tool	TANGENTIAL_BLADE
Spindle Speed	2000
Spindle Direction	CCW
3. Process	
Depth Increment	3
Sum of Increments	3
Plunge Feedrate	3000
Cut Feedrate	3000
Rapid Feedrate	4000
Height of Clearance Pla	8
Milling Direction	CCW
Working plane	0
4. Lead Moves	
Diving Ramp	0
Lead Radius In	0
Lead Radius Out	0
5. Tool	
Radius Correction	NONE
Type of Radius correcti	NORMAL
Tool Ident	Tangential Blade
8. Drag Knife	
Activation Angle	5
Rotation Feedrate	3500
9. Special	
Offset	0

Figure 56. 2D Section: Parameter of G-code [From GrblGru]

will be generated from the drawing, Fig. 60.

- **Toolbar:** This is a strip of buttons that allows users to perform common tasks, such as zooming in and out, panning the drawing, and selecting different tools, Fig. 60.

- **Status bar:** This is a strip at the bottom of the control panel that displays information about the current drawing and the software's status. It may include information such as the current layer, the current tool, and any messages or warnings, Fig. 60.

- **Command bar:** In this section you can send specific commands to carry out for

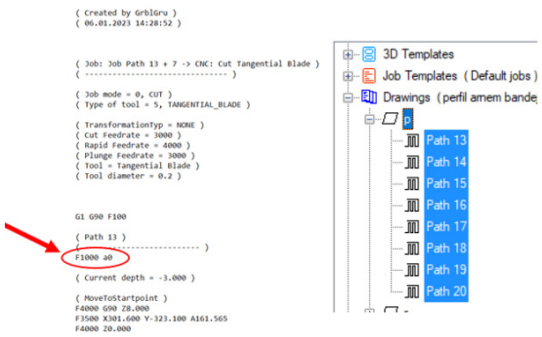

Figure 57. G-code [From GrblGru]

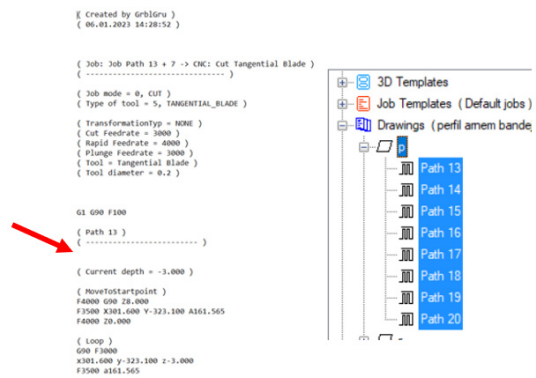

Figure 58. Final G-code [From GrblGru]

the CNC. Normally it is used to verify the correct operation of the machine, Fig. 60.

- **Macro side panel:** This is a panel on the side of the control panel that includes various controls and settings for the software. It may include options for adjusting the feed rate, tool size, and other machine settings, as well as buttons for generating and exporting G-code, Fig. 60.

Once the g-code generator is done, the product preview appears in 3D next to the CAD model of the example CNC Fig. 61.

5.6. Custom Macro Setting for CNC Drag Knife

The custom macro settings in GRBLGru allows to define custom commands or sequences of commands that can be executed from the GRBLGru interface or included in G-code programs.

The custom macros in the GRBLGru settings menu can be setted by specifying the

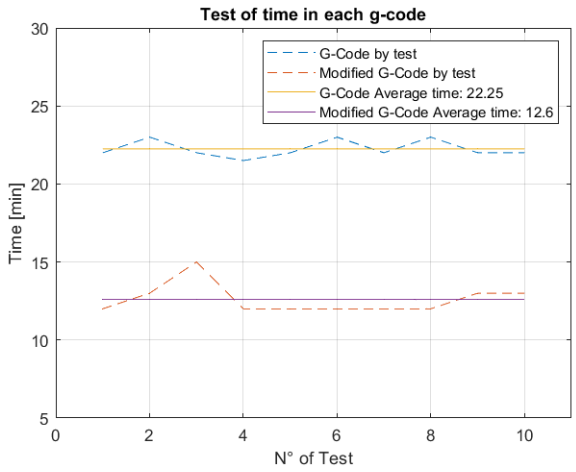

Figure 59. Average time of G-code cases [Made in Matlab]

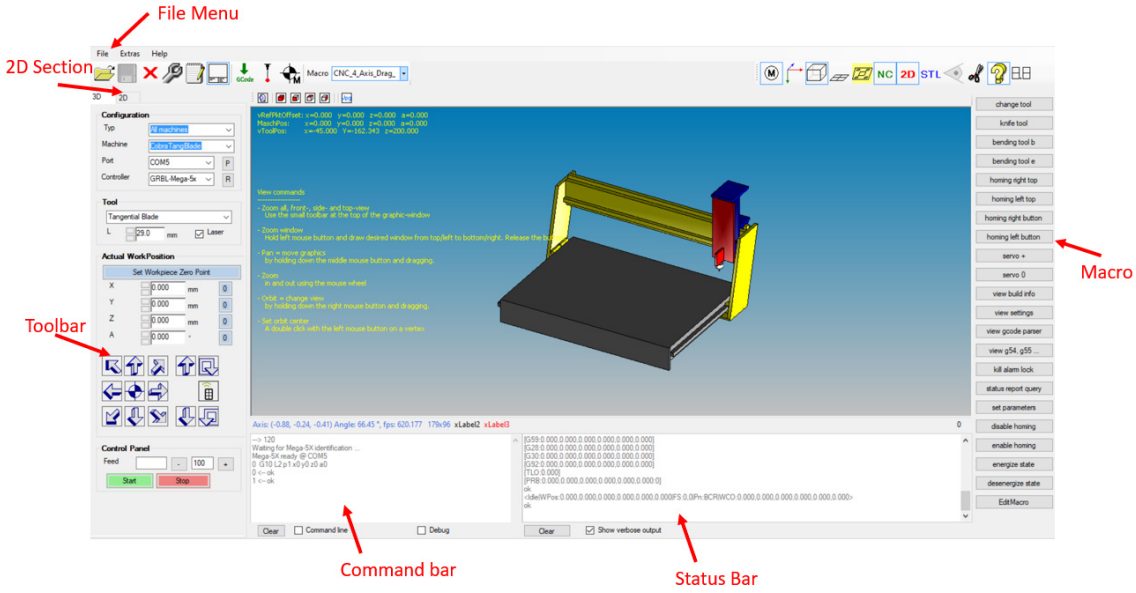

Figure 60. GrblGru Control Panel [From GrblGru]

name of the macro and the G-code commands to execute. Then the user can use the custom macro by entering the macro name followed by any necessary arguments in the command input field of the GRBLGru interface, or by including the macro name and arguments in G-code programs, Fig. 61.

- **Change Tool:** This custom configuration allows to establish the necessary commands for the program to zero the axes and allow to change the tool from bending to cutting or vice versa.

- **The knife tool and the bending tool b and e:** this command allows to set the tip of the tool on plane 0, which is the height at which the cardboard plate is located,

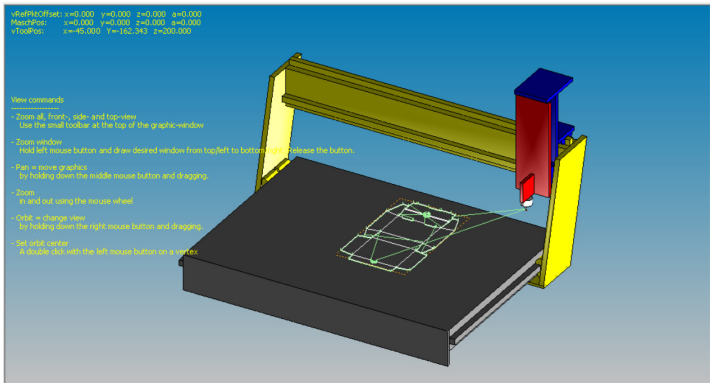

Figure 61. GrblGru Control Panel: Product ”Postre Box” [From GrblGru]

as shown in the Fig. 62.

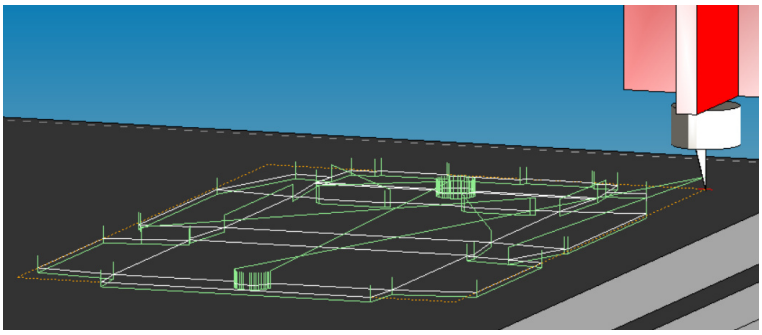

Figure 62. The knife tool position [From GrblGru]

- **Homing ”Right Top”, ”Left Top”, ”Right Button”, ”Left Button”:** This command allows to establish the homing of the CNC in the four corners of the machine, this because it depends on the application and the size dimensions of the product to only occupy a specific section of the base.

The rest of the Macro configuration is to verify the operation of the CNC parameters within the GrblGru environment.

5.7. CNC Control Diagram

Once the software has been implemented and the connections made in the microcontroller, the CNC control process is fundamentally based on the interface provided by the GrblGru software with its integration of 3D visualization, G-code generation, control panel and configuration control ” Macro” to determine g-code commands which will be

interpreted in the Arduino Mega to send the require pulses to each stepper driver to control the behaviour of each motor to achieve the desired position. This process is presented in Fig. 63.

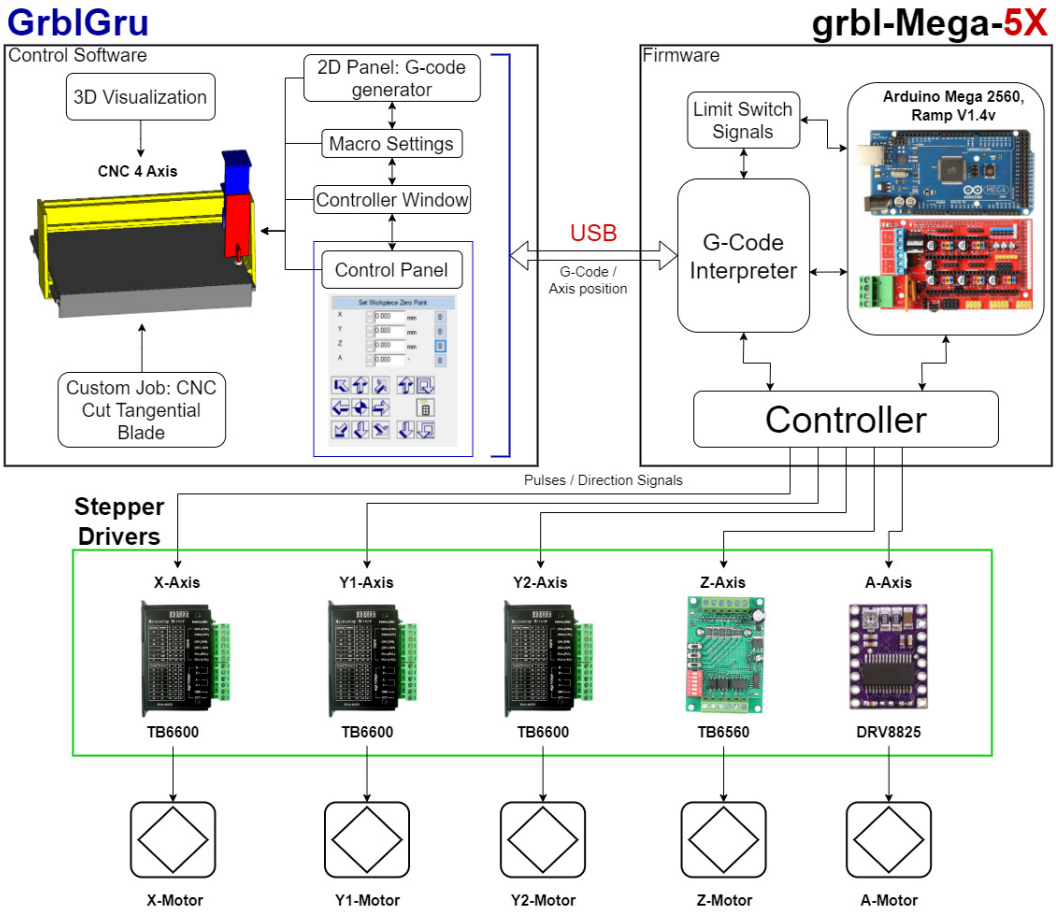

Figure 63. CNC Control Diagram [Made in Drawio]

6. Bending and cutting process

The general process is subdivided into two: the bending process and the cutting process, for each process a specific tool is used as shown in Fig. 64. The cutting process requires a force of 20.76 N, equation 15, with the proposed design also seen in Fig. 10, while on the other hand the bending process requires a slight bump on top of the cardboard plate to mark the bending path, this is due to because once the box is made, a manual pre-bending is required in all box manufacturing processes. This pre-bending is done when the box is already with the customer at the time it is used for the ultimate purpose. For this reason, the design for the tool are shown in Fig. 64.

It should be clarified that the design of the box is provided by the company already in a DXF file.

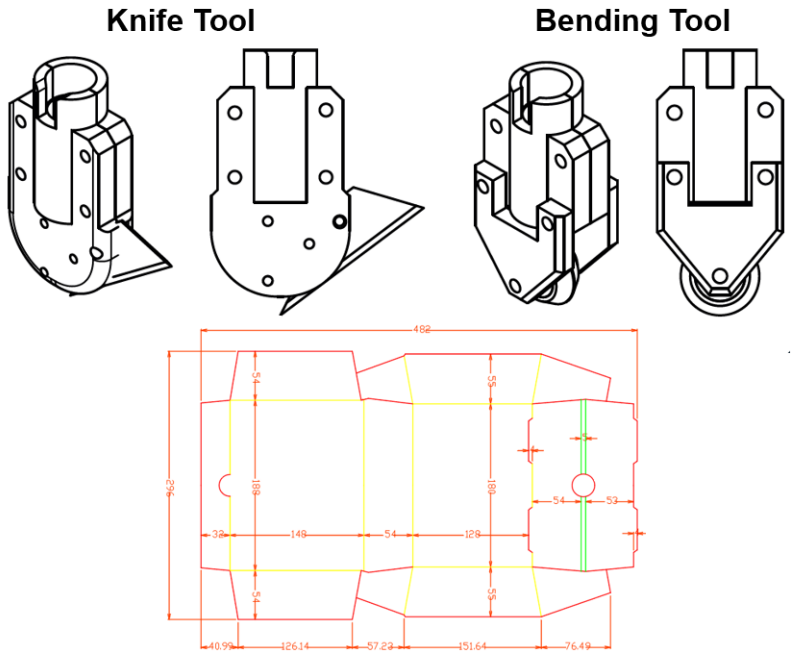

Figure 64. Knife and bending tool [Designed in Inventor]

In the same Fig. 64 the two tools are observed, however, the colors of the lines determine which one is going to be used:

- **Bending tool:** yellow and green lines
- **Knife tool:** red lines.

In the Fig. 65 the finishing of the two threads is shown, resulting in the final ”Postre box” product.

7. Artificial Inteligence

Artificial intelligence is carried out through semantic segmentation image classifier in combination with object detection and dimensions measurement to ensure the bending and cutting process were correctly made.

7.1. AI Azure Image Classifier

Once the box´s fabrication process is acomplished, the software is induced to capture a image and send it to an already trained IA Image Classifier to verify if the box is

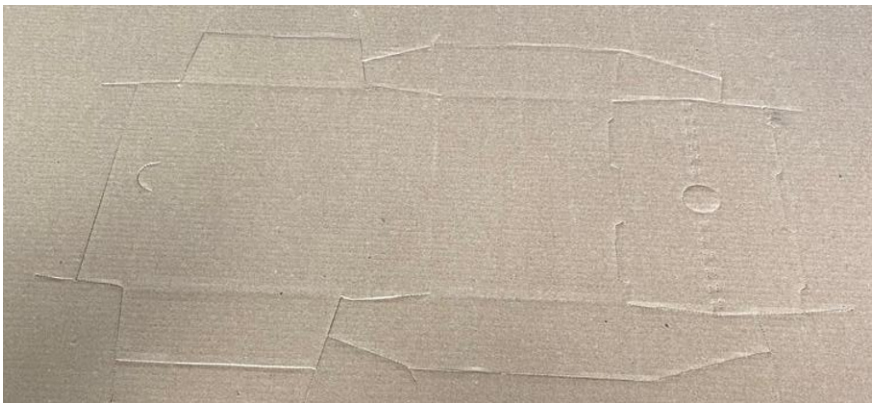

Figure 65. Finished bending and cutting process of ”Postre Box”

already cutted or not. This is a web Service called Azure from microsoft, which allows to codifique and train an AI, keep it online, and be able to recieve feedback by an IP address connected to an executable. [28]

The service is based on an API generated once the model is trained with the set of images necessary to establish a cut final product relationship. As is shown in Fig. 66

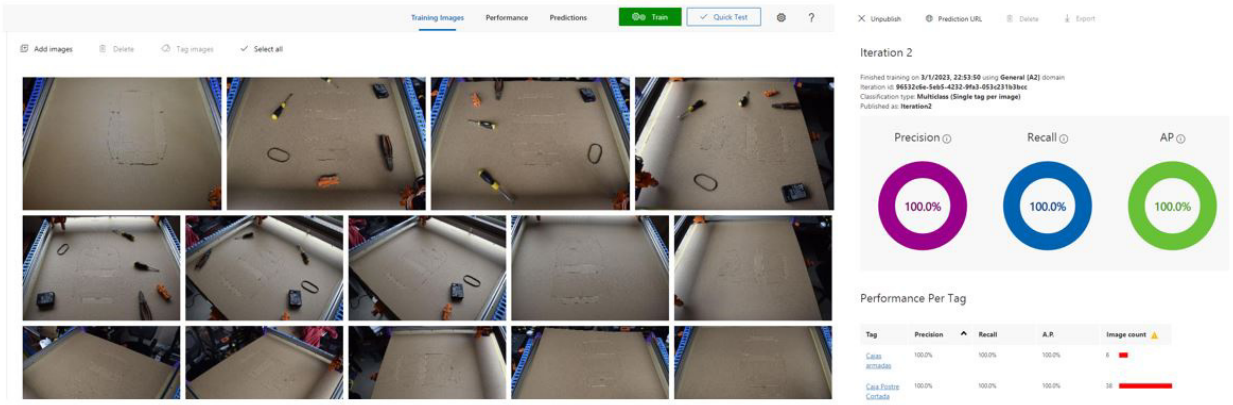

Figure 66. Image classifier: Trained Model [Made in Azure Service]

Once the connection has been completed, the code can be integrated as a java script ”.js” file which will allows to use the API and connect to the server as shown in Fig. 67. [29]

In this way, the Azure service provides a URL with a prediction key code, seen in Fig. 67 (await Fetch function) that allows connection and verification of the image.

The step for the verifications consists mainly in:

- **Box finished:** In this step, the completion of the manufacturing process is iden-

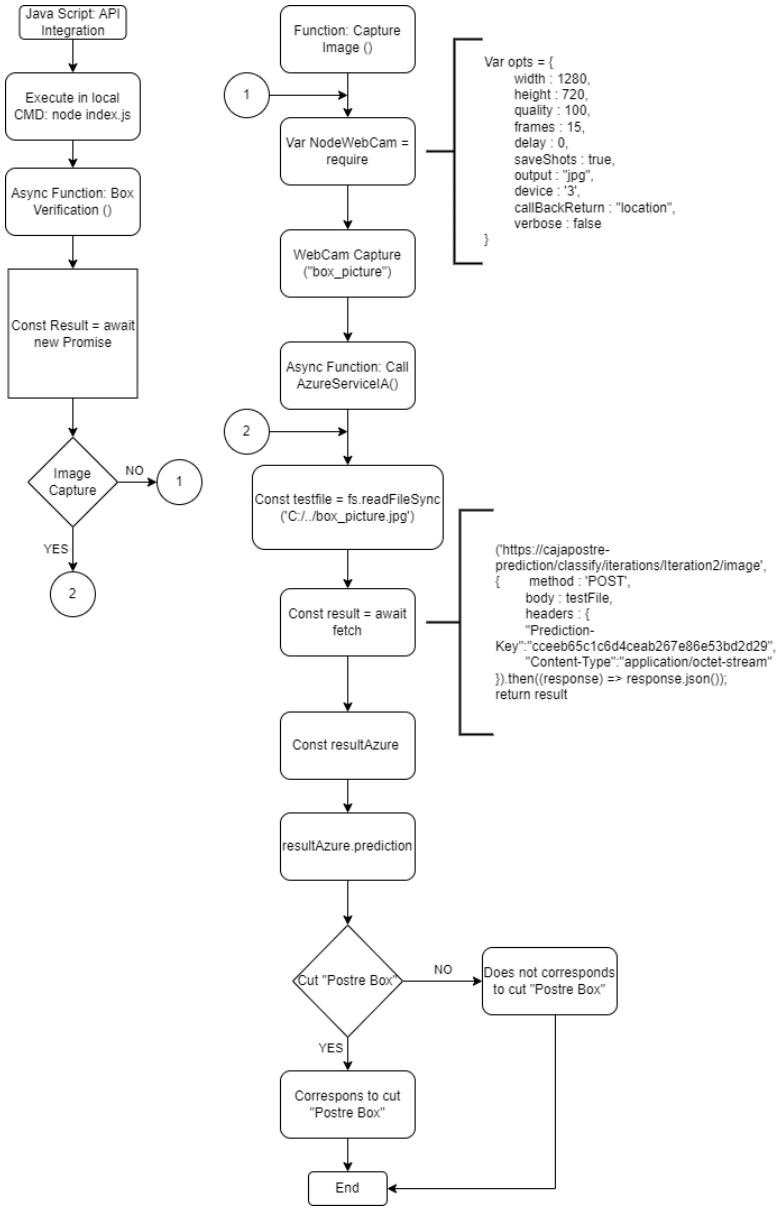

Figure 67. Flowchart: API Integration to command window through a java script file ”node index.js” [Made in Autocad]

tified and a link is established with the API address to activate the image classification process of the Azure service, Fig. 68.

- **Cutting and box verification:** The Azure service classifies the image and sends a response with a probability percentage to determine which type of box is already cut, Fig. 69.

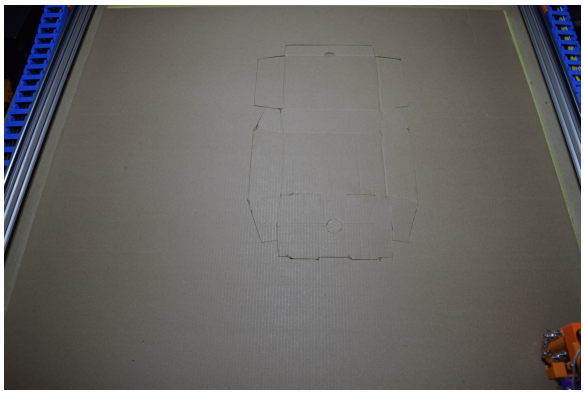

Figure 68. Box finished [Taken by top view camera]

```
C:\Users\ricar\Desktop\Tesis_IA>node index.js
(node:16420) ExperimentalWarning: The Fetch API is an experimental feature. This feature could change at any time
(Use `node --trace-warnings ...` to show where the warning was created)
result {
  id: '9b55420f-06f5-49cc-8c40-e9f895594fb3',
  project: 'ece281c3-ba5e-4199-8c39-10d6a87d7cd8',
  iteration: '96532c6e-5eb5-4232-9fa3-053c231b3bcc',
  created: '2023-01-05T21:22:05.360Z',
  predictions: [
    {
      probability: 0.99980766,
      tagId: '66b4c63c-9e66-4c7d-971d-4f4ed2707a88',
      tagName: 'Caja Postre Cortada'
    },
    {
      probability: 0.00019237658,
      tagId: 'aaa057ff-037d-4fc6-b46f-306ace66d1bf',
      tagName: 'Cajas armadas'
    }
  ]
}
Corresponde a Caja Postre Cortada
```

Figure 69. Cutting Verification [From local CMD]

Iterations and Probabilities Test

The environment of the images was considered as shown in Fig. 66, where only the plate with the box already cut and its environment surrounded by random objects is established. Then for the training of the image classifier model, the following parameters must be taken into account:

- **N° Images Box:** is the quantity of images which contain the desired box, in this parameter the tarjet aims to avoid the ”overfitting” problem which appears when the image is ”ideal” and there is no other noise or extra objects that could affect to defect the desired box. So the solution is simple, the images must not only have the desired object, but also extra random objects that fulfill the noise function.
- **N° Images Random Object:** in this parameter, a separate label must be placed

within the image classifier so that if the classifier detects that it does not meet the requirements, that is, it does not contain a box within the image, then it will classify it within this label, called ”random object”, the number of images for this parameter is set to be 30% of the iteration batch.

- **Training time:** This parameter is the result of the training time invested in each iteration, measured in minutes.
- **Probability threshold:** This parameter is chosen to be reached as the maximum precision for each iteration.
- **Probability validation:** This parameter describes the probability resulting from each iteration that was evaluated with a random image from the training set. It should be noted that the objective is for this parameter to reach the desired value of the threshold probability.

The desired validation probability value of 0.99 was reached in iteration number 19, with 575 images of cardboard boxes and 173 images with random objects, as seen in Fig. 70 and Fig. 71.

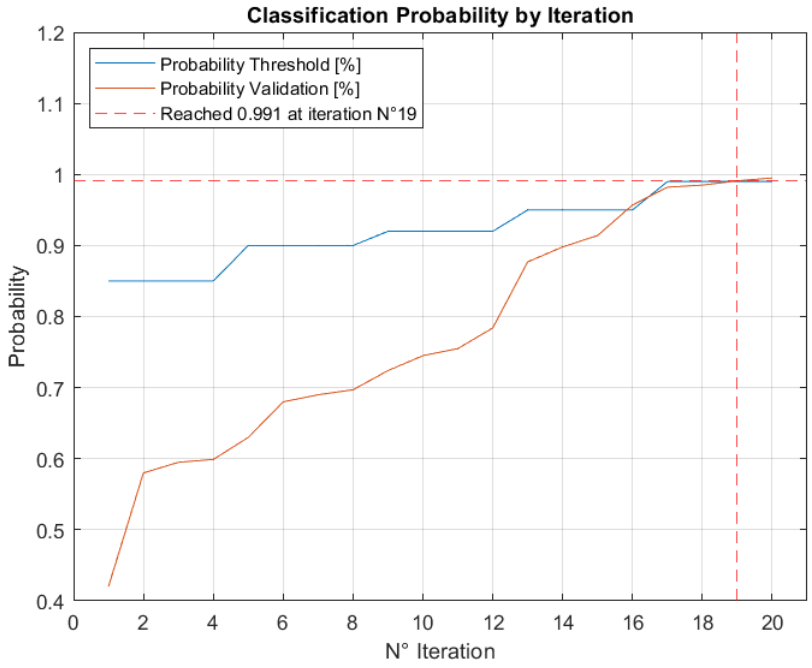

Figure 70. Classification probability by iteration [Made in Matlab]

Table 11. Iterations and Probabilities Test

Iteration	N° Images: Box	N° Images: Random Object	Training Time [min]	Probability Threshold [%]	Probability Validation [%]
1	22	7	12	0,85	0,42
2	37	12	17	0,85	0,58
3	41	14	23	0,85	0,595
4	49	16	29	0,85	0,599
5	55	18	31	0,9	0,63
6	123	41	62	0,9	0,68
7	168	55	82	0,9	0,69
8	204	67	105	0,9	0,697
9	236	78	127	0,92	0,724
10	278	92	182	0,92	0,745
11	325	107	207	0,92	0,755
12	355	117	234	0,92	0,784
13	380	125	255	0,95	0,877
14	402	133	286	0,95	0,898
15	436	144	314	0,95	0,914
16	461	152	335	0,95	0,957
17	490	162	357	0,99	0,982
18	541	179	396	0,99	0,985
19	575	190	401	0,99	0,991
20	589	194	428	0,99	0,995

Similarly, the corresponding training time for iteration No. 19 can be seen in Fig. 72 with a value of 401 minutes or 6.68 hours.

The use of 575 images of the desired object in conjunction with images of the random object that serve as a discarded probability label allows establishing a training relationship for the model in iteration number 19, reaching from this point the probability of success of 0.99 or 99% for the AI to determine and classify if the object is a cut card or not.

7.2. Object detection and dimensions measurement

The object detection is carried out with an ”aruco” marker, which are fiducial square dimensional markers used for camera angle and coordinates pose estimation. An ”aruco”

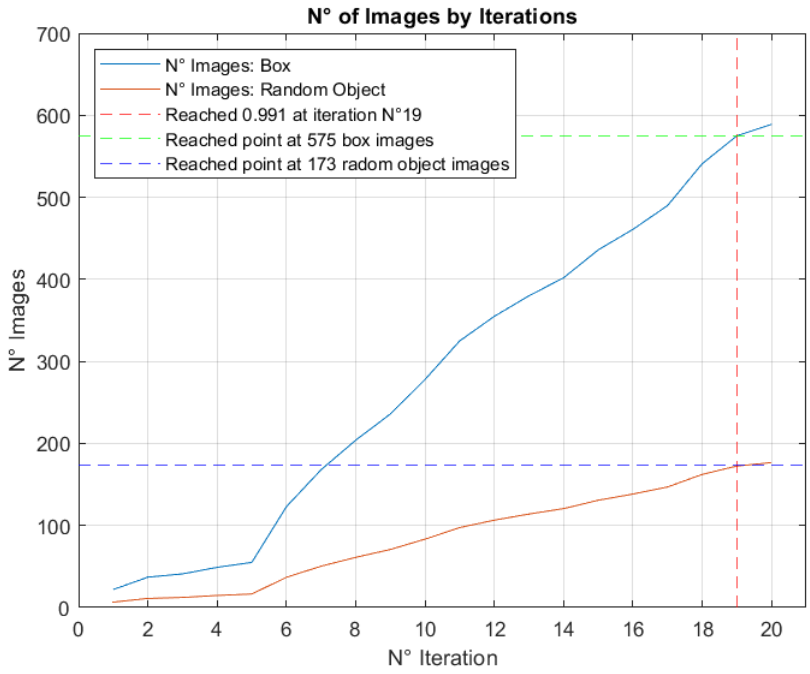

Figure 71. N° of images by iterations [Made in Matlab]

marker is in concept a defined symbol with symetric square profile which in its inner space has a binary matrix enclosed within a wide black color border with a determine indentifier. [30]

The dimenions of the inner binary matrix are determined by the marker. The structure of the odd patron represent the parity bits meanwhile the even blocks shows the data bits. Its simple functinality is composed by the black border to facilitate a fast detection of the main object and the binary design determines its identification. The tarjet is to help the camera to understand the angle, height, and depth and has its application in computer vision. The process has three main step:

1. **Step 1:** detect the aruco marker in the image inside of the overview panoramic image, then calculate the pixel to centimeter conversion ratio with the known perimeter for the aruco marker, in this case 5x5 cm.

2. **Step 2:** compute the object size based on the object coordinates and the pixel to centimeter conversion.

3. **Step 3:** define and locate the object limits according to its computed size.

This is called image processing as the last AI subprocess that allows to recognize

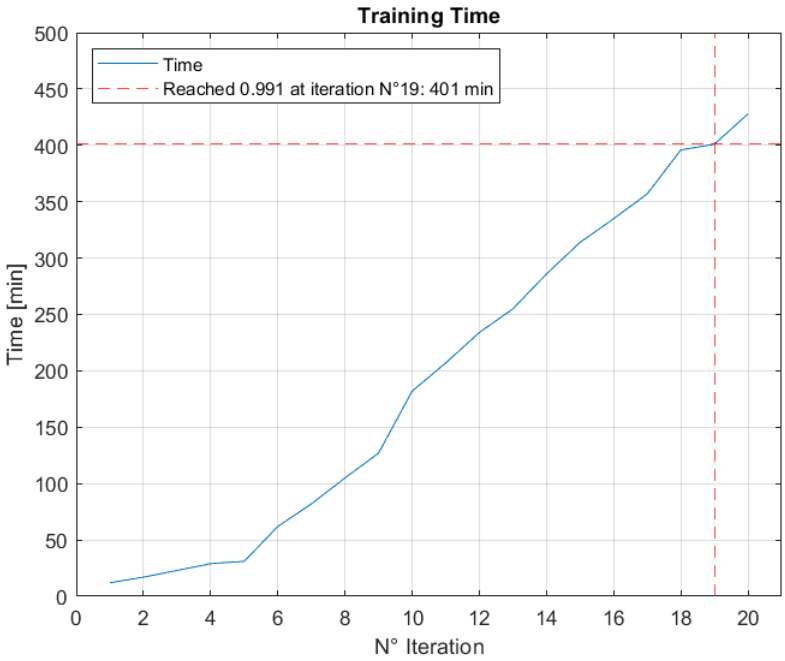

Figure 72. Training time by iterations [Made in Matlab]

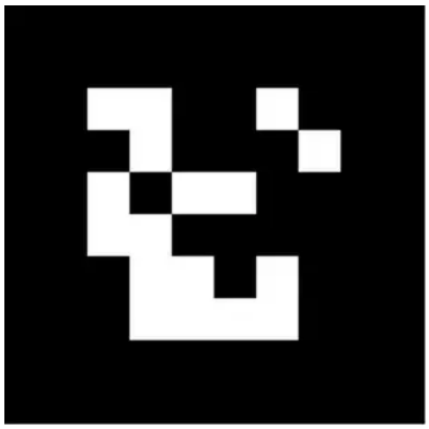

Figure 73. Aruco Marker [9]

objects and take a measurement of the captured object from an ”Aruco” maker [31]. The following Python code shows is functionality. Fig.74 .

Dimension Test

The dimension tests were carried out following the ”Postre Box” protocol for its manufacture, and then its dimensions were verified.

In the Fig. 76, the behaviour of the IA object detection is created and verified with each total error, it can be said that the detection remains in nearly of the real contants of the box. The global error is given by the global mean in Table 12 as:

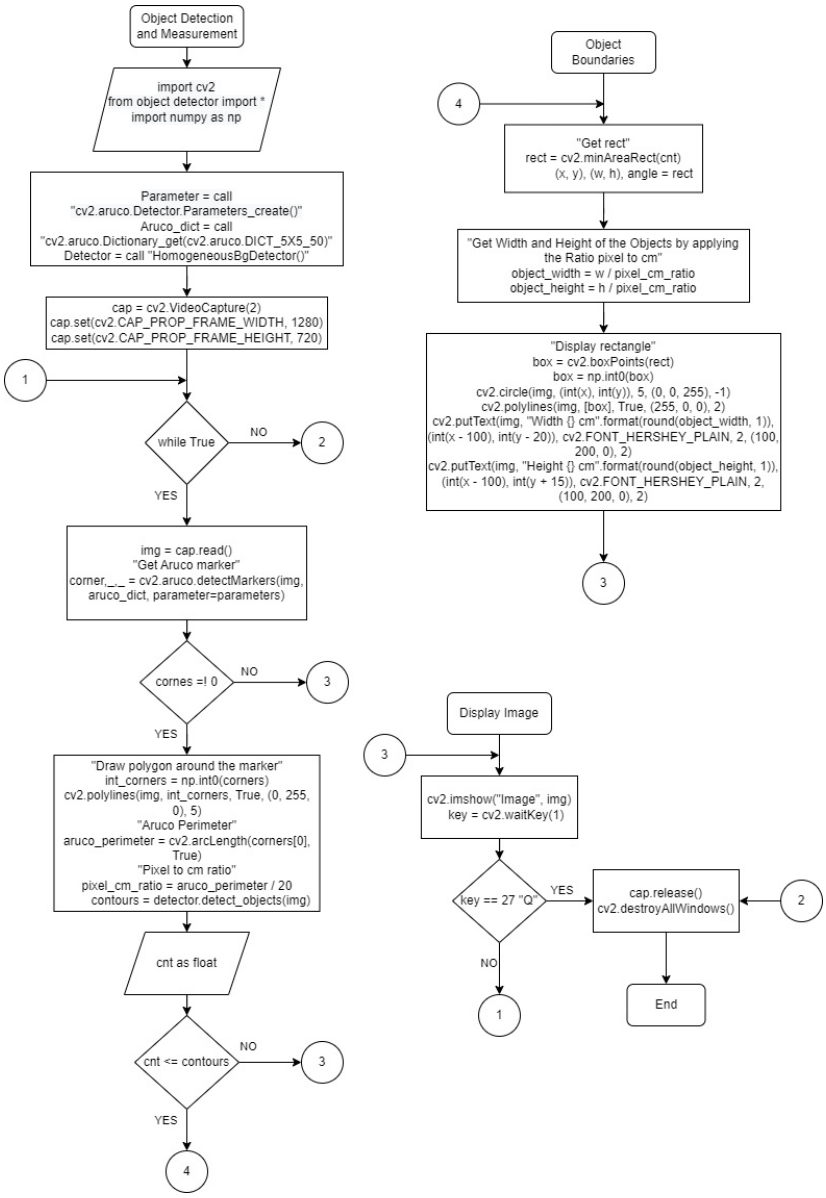

Figure 74. Flowchart: Python Integration Object detection and measurement [Made in Autocad] [10]

$$Error_{dimenion} = \frac{6.55 + 7.22}{2} = 6.88[\%] \tag{86}$$

7.3. AI and object dimensions measurement process

Once the two threads have been described, their implementation can be seen in the block diagram of Fig. 77.

The process is categorized into the following steps according to Fig. 77.

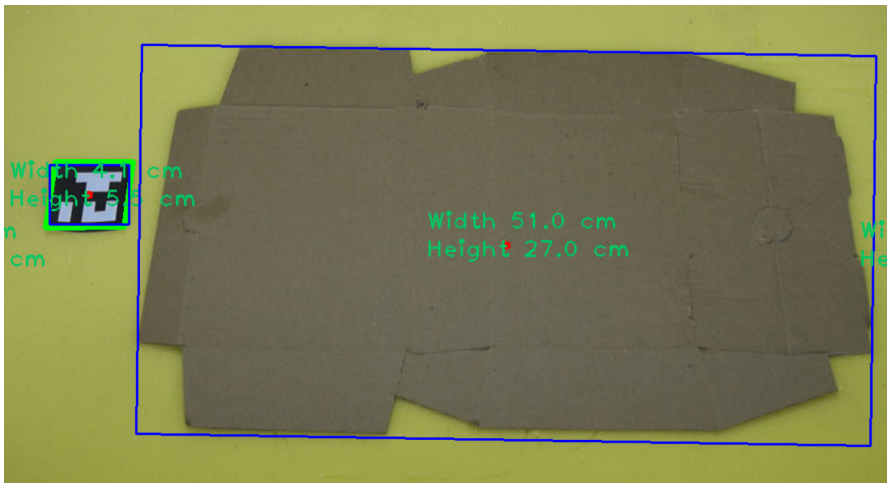

Figure 75. Cutting Dimensions Verification: Postre Box [Taken by top view camera]

Table 12. Dimensions Test

Test	Real W [cm]	Calculated W [cm]	Error [%]	Real H [cm]	Calculated H [cm]	Error [%]
1	48.2	51.0	5.81	29.6	27.0	8.78
2	48.2	46.0	4.56	29.6	30.8	4.05
3	48.2	47.5	1.45	29.6	28.5	3.71
4	48.2	50.5	4.77	29.6	31	4.72
5	48.2	46.8	2.91	29.6	26.3	11.14
6	48.2	49.0	1.65	29.6	27.7	6.41
7	48.2	50.9	5.61	29.6	27.0	8.78
8	48.2	51.2	6.22	29.6	27.0	8.78
9	48.2	49.6	2.91	29.6	28.0	5.41
10	48.2	50.0	3.73	29.6	26.5	10.47
		Total:	**6.55**		**Total:**	**7.22**

- **Step 1:** Application to capture the image.
- **Step 2:** Image capture via camera web and storage the data in real time.
  - Step 2.1: Data image transcribed to the java script integration to begin the API connection.
  - Step 2.2: Data image transcribed to python integration to begin the image processing.
- **Step 3:** Obtained image data and setting the hyperparameter for the java integration via a ”node index.js” file.

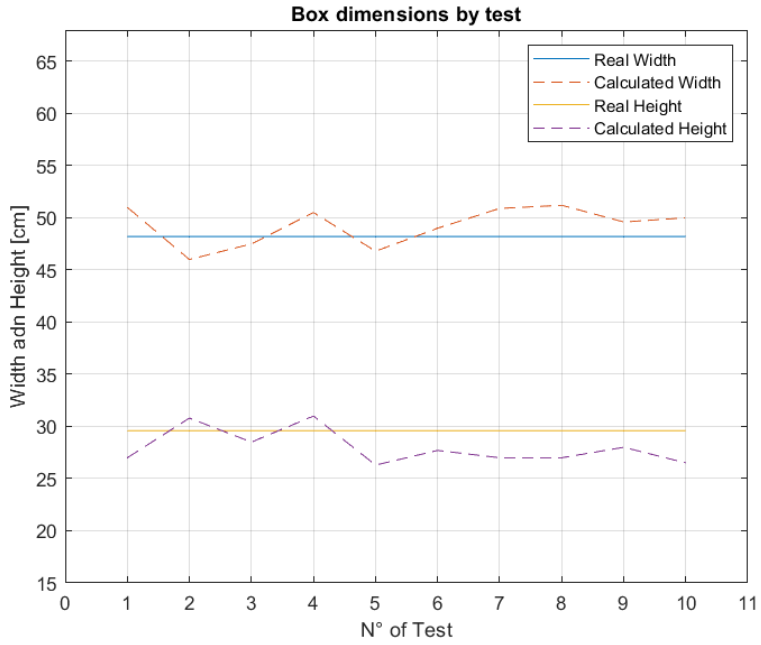

Figure 76. Cutting Dimenions IA Behaviour [Made in Matlab]

- **Step 4:** Sending the image pre-processed data to the cloud ”API processor”.
- **Step 5:** Start the computer vision API via Custom and computer vision configuration with pre-trained model ”Semantic segmentation” from Azure service.
- **Step 6:** Classification by iterations within a margin error of 1% according to the pre-trained model until set and reach the managed endpoint of the machine learning.
  - Step 6.1: The training loop begins with tha data storage of the cloud service.
  - Step 6.2: Tha image data probabilities is send to the azure analytics iteration to verified the classification of the cardboard box with the already data of previous iterations.
  - Step 6.3: Meanwhile at the same time the data probabilities is used for a new subrutine of the iteration as second verification process.
- **Step 7:** Send the image real time data probability of classification to the local Java script integration in the CMD windows.
- **Step 8:** Represent the probability classification in the application CPU with the API client, as seen in Fig. 69.

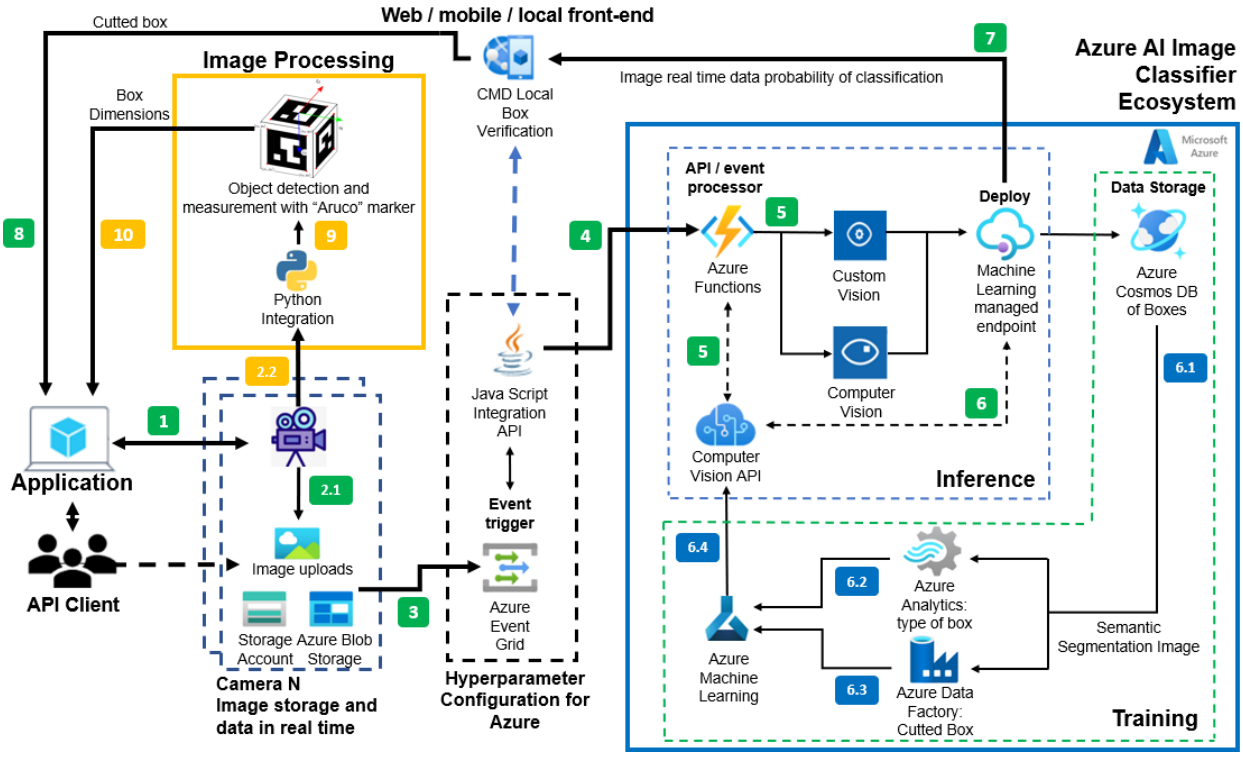

Figure 77. Block Diagram: AI Azure and Image Processing for Cardboard Boxes verification [Made in Azure Microsoft Visio]

- **Step 9:** Verify and locate the dimensions coordinate of the ”aruco” maker on the overview of the image according to its binary matrix to determine the size of the nearest object (already cut box) in the capture.
- **Step 10:** Represent the box dimensions in the application CPU with the API client, as seen in Fig. 75.

In this way, it is verified that the cut verification AI with image processing for routing dimensions in the object, in this case, ”Postre Box”, is effective with an error rate of 6.88 %. According to the error pattern it can be said that one of the causes of this is the change of light exposure in the product, which determines if the detection of the box is correct or not. It is recommended that for future tests, image detection and processing be performed under ideal lighting conditions.

8. Operation Flowchart

The flowchart in Fig. 78 presents the operation process of the CNC machine in conjunction with the product analysis AI.

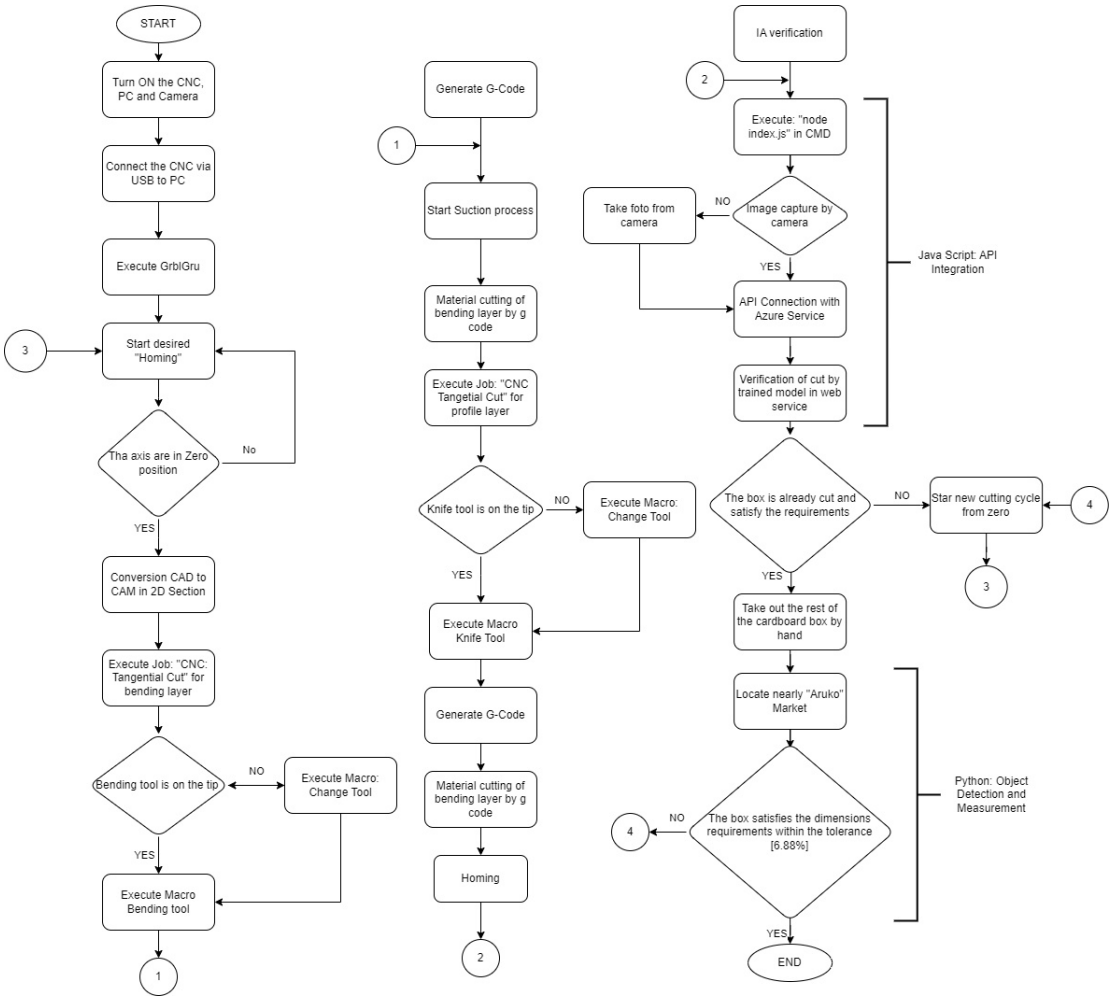

Figure 78. CNC´s Flowchart [Made in Autocad]

The manufacturing process of the ”Postre box” once configured and chosen the work to be carried out in the GbrlGru software, as seen in section ”Control software”, the sub processes of bending and cutting of the box are established, once the CNC operation is finished, the AI verifies if the desired box is already cut through the Azure service image classifier and later its dimensions are verified by image processing through the aruco marker, as can be seen in Fig. 77. Then once the pre-bending manual process is made at the moment it is gonna be used, the final product is the box, as shown in the Fig. 79.

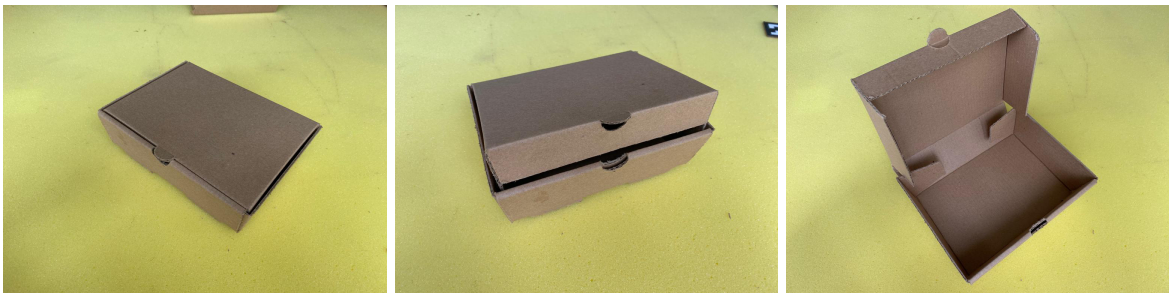

Figure 79. ”Postre Box” finished

9. Component Manufacturing

9.1. 3D Printing

The process call ”3D printing” depends on creating physical objects by layer addition per step from CAD models. It is also known as additive manufacturing, because it involves adding material to create an object [32], rather than subtracting material as in traditional manufacturing processes such as machining or casting.

In 3D printing, a digital model of the object to be printed is created using computer-aided design (CAD) software. This model is then sliced into thin layers and the 3D printer creates the object by depositing successive layers of a building material, such as plastic, metal, or ceramic, in accordance with the digital model. [33]

For the manufacture of custom components not purchased in the market, the manufacture by plastic deposition ”3D Printing” was used with the bio-polymer known as PLA (Polylactic Acid), with the following characteristics in Table 13:

Table 13. PLA Properties [11]

Physical Propoerties	PLA	Units
E	0.35 - 3.56	GPa
E*	0.28 - 2.81	kNm/g
$\wp$	1.2 - 1.245	g/cm^3
σ	20 - 60	MPa
σ^*	16.9 - 48	MPa
T_g	45 - 60	℃
T_m	150 - 162	℃
ϵ	2.2 - 6	%

The table 14 shows all the pieces printed in 3D, the number of filaments in grams used per piece and their printing time.

Table 14. 3D printed components

Component	Quantity	Filament [gr]	Subtotal Filament [gr]	Print Time [min]	Total Print Time [min]
Holder Chain	2	8,19	16,38	27	54
Holder Chain End	2	5,33	10,66	20	40
Holder Knife	2	13,93	27,86	47	94
Shaft A guide	1	39	39	96	96
Base Z	1	27,58	27,58	73	73
Nema 17 Holder	1	24,34	24,34	82	82
Base Servo	1	4,92	4,92	21	21
Case Hall	1	3,74	3,74	18	18
Z Vertical Base	1	39,35	39,35	118	118
Corner Bed	4	100,36	401,44	177	708
Corner Support	8	25,52	204,16	65	520
Holder Camera	1	58,42	58,42	215	215
Limit Z Holder	1	1,87	1,87	11	11
Limit X	2	4	8	14	28
Holder 1	1	35,97	35,97	104	104
Holder 2	1	45,71	45,71	129	129
Right Lateral	1	164,11	164,11	291	291
Left Lateral	1	157,74	157,74	290	290
Contrary Holder Y	2	29,52	59,04	76	152
Holder Chain X	1	10,31	10,31	51	51
Nema Separator	4	0,67	2,68	5	20
X and Z Support	1	95,59	95,59	265	265
Top Z	1	25,53	25,53	77	77
Timing Belt Adjuster	4	3,71	14,84	22	88
Limit Y	4	10,72	42,88	32	128
	Total:	**1522.12**		**Total:**	**3673**

The total filament used corresponds to a value of 1522.12 grams as shown in the table 14, which corresponds to a roll of PLA filament and half of another, this because within the market the filaments are sold per roll, which is equivalent to 1 kilogram. On the other hand, the total printing time for the pieces is around 3673 minutes, or 61.2 hours.

With the total hours used for 3D printing, and knowing that Ecuador's national KWh rate is $0.092 [34] and the average power consumption of a 3D printer is 150W [35], the total cost of electricity consumption can be established with the equations 87 and 88 [36]:

$$E = P * t * \frac{KWh}{1000W} = 150" * 61.2h * \frac{KW}{1000W} = 9.18\ KWh \tag{87}$$

$$Cost = E * \frac{\$0.092}{KWh} = 9.18KWh * \frac{\$0.092}{KWh} = \$\ 0.844 \tag{88}$$

It is thus that the total cost given by the electrical consumption for the manufacture of the 3D parts surrounds the value of $0.84.

9.2. Wood routing

Wood routing with a CNC machine involves using a router to cut, shape, or carve wood into a specific design or shape degrading the material layer by layer until reach the desired heigh [37]. CNC routing allows for precise and repeatable cuts and shapes to be made in wood and other materials. For the routing, the design of the Fig. 80, 25 mm thick MDF was used due to its low manufacturing cost, ans it was sent to an external CNC Milling company.

A simple example of the dimensions of the routed base is presented in Fig. 80 and its main mechanical properties in table 15.

Table 15. MDF Properties

Physical Propoerties	25 mm Thick	Units
Density	730	Kg/m^3
Tensile strength	0.75	N/mm^2
Flexural strength	30	N/mm^2
E	2300	N/mm^2

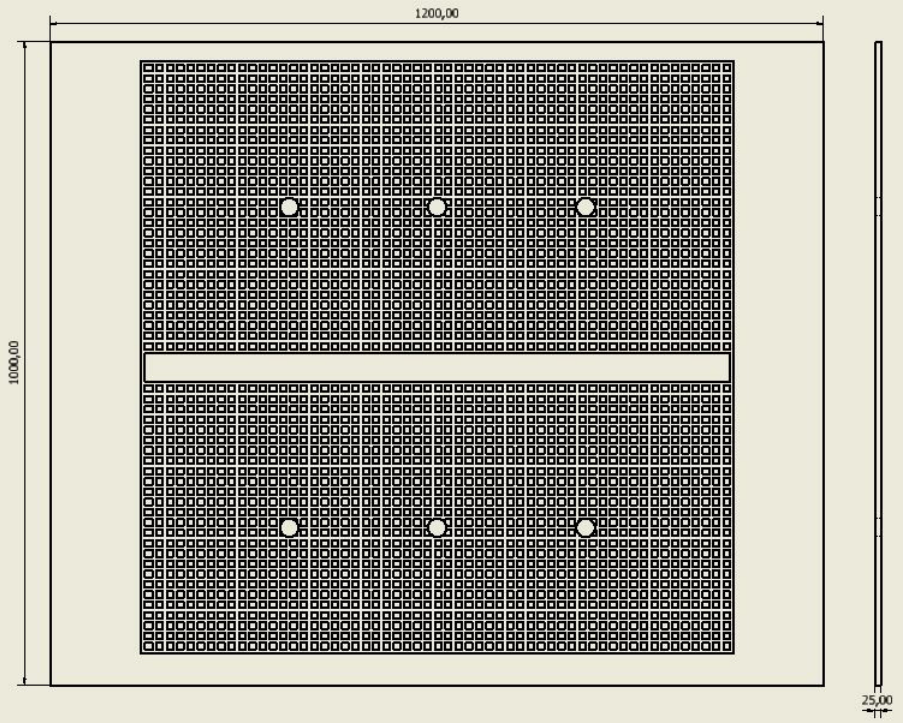

Figure 80. Routed Base [Designed in Inventor]

10. Costs and standardization of components to the market

The acquisition of materials and components was a process where the standardization of the Ecuadorian market was taken into account, seeking benefit-quality prices that meet the requirements of each component, so the following tables present an estimate of the important components of the project.

Sellers:

1. Innovatech
2. Electronics Ec.
3. Robotics
4. Perfiles CNC
5. Material Electronico
6. Ecuador Masis
7. Electronica del valle

8. Megatronica

9. James Import

Table 16. Mechanical Components

Component	Features	Vendor	Price	Qnty	Total Price
Polea	20 teeth, 8mm	1	$ 4.70	2	$ 9.40
Flexible coupler	8-8mm	2	$ 2.99	2	$ 5.98
Rodamiento Lineal	8mm, SC8UU	2	$ 5.45	4	$ 21.80
Rodamiento	608RS 8mm	3	$ 2	2	$ 4
Threaded bar	8mm, 2mm pith, 30cm	2	$ 6.55	1	$ 6.55
Threaded bar	8mm, 4mm pith, 100cm	4	$ 21.00	1	$ 21.00
Steel bar	8mm, 30cm	4	$ 4.50	2	$ 9
Steel bar	8mm, 15cm	4	$ 2.30	2	$ 4.60
Metal Corner	4mm, 2 mm	5	$ 0.80	4	$ 3.20
C Beam kit V slot	40x40 double base	4	$ 97.00	1	$ 97.00
Bar motion nut	Anti-backlash block 8mm	4	$ 8.60	1	$ 8.60
Alumium Extrusion	20x20mm T-slot, 100cm	3	$ 10	7	$ 70
Alumium Extrusion	45°, 20x20mm T-slot, 50cm	3	$ 5	4	$ 20
Alumium Extrusion	20x40mm T-slot, 100cm	3	$ 17.50	4	$ 70
Alumium Extrusion	20x40mm V-slot, 100cm	4	$ 16	3	$ 48
Alumium Extrusion	C beam, 40x80x1000mm	4	$ 36.10	1	$ 36.10
Wood Bases	Routed bed 1040x1000mm	6	$ 34	1	$ 34
Wood Bases	Frame bed 1040x1000mm	6	$ 13.40	1	$ 13.40
PU Foam	12CN 95% Porosity, 2x1m	9	$ 4.50	1	$ 4.50
PLA Filament	1.5kg	3	$ 30.0	1	$ 30.0
				Total:	**$ 548.12**

The total cost of the project rises to a figure of $ 1625.31. This undoubtedly underlies the estimated cost of a CNC with this capacity of tangential knife with the same dimensions within the available market, being from $5,000 to $8,000.

Table 17. Electronic Components

Component	Features	Vendor	Price	Qnty	Total Price
Nema17	12V,2A,1.8°	3	$ 16.50	1	$ 16.50
Nema23	24V,2.8A,1.8°	2	$ 46.26	3	$ 138.78
Nema23	24V,4.2A,1.8°	2	$ 87.75	1	$ 87.75
Servo MG996r	6V,0.9A	2	$ 12.0	1	$ 12.0
Driver	TB6600, 1/32,0.8A	2	$ 27.50	3	$ 82.50
Driver	TB6560, 1/32, 0.5A	2	$ 15.20	1	$ 15.20
Driver	DRV8825, 1/32, 0.5A	2	$ 4.50	1	$ 4.50
Cable	Plug cable 110V AC	7	$ 8.50	1	$ 8.50
Cable	USB B-USB A extender	8	$ 7.50	1	$ 7.50
Protection	Fuse 20A	7	$ 2.40	1	$ 2.40
Protection	Fuse holder	7	$ 0.50	2	$ 1
Source	DC Power supply 24V 20A	2	$ 20	1	$ 20
Volage regulator	7805, 1A	7	$ 2.50	1	$ 2.50
Microcontroller	Arduino Mega 2560	8	$ 29.50	1	$ 29.50
Cable	Mini HDMI- HDMI, 5m	8	$ 7.50	1	$ 7.50
Cable	Video capter	8	$ 12.5	1	$ 12.50
Cable	Concentric 4X16, 1m	5	$ 0.40	4	$ 1.60
Cable	Concentric 4X18, 1m	5	$ 0.38	7	$ 2.66
Cable	Wire 22 AWG, 1m	5	$ 0.25	12	$ 3
Minor componentes	Capacitors, connectors, etc	8	-	-	$ 17.46
Cabinet	40x30x25cm	5	$ 53.0	1	$ 53.0
Power Conmsuption	Energy consumption for 3D printing	1	$ 0.844	1	$ 0.844
Suction Vacuum	110 V, 1800 RPM, 1100 W	1	$ 250	1	$ 250
Camera Nikon	D5300, 1080X720, 60FPS	1	$ 300	1	$ 300
				Total:	**$ 1077.19**

11. Conclusions

- The process carried out made it possible to establish a direct optimization relationship for the manufacture of boxes, this is because normally a cardboard

company only produces boxes wholesale, because its processes are designed to be only profitable when its production is wholesale.

- Likewise, the use of four control axes for the cut, meant a more precise and faster manufacturing when cutting compared to if it had been done manually. The ”Postre Box” normally has a manufacturin time of 150 minutes if it is done by hand, but know with the CNC it is reduced to 15 minutes.

- This feature was possible thanks to the implementation of the free software called ”GrblGru” that allowed the proper customization of the g-code and the macro control commands for this CNC.

- The AI was able to correctly verify, within its margin of error of 6.88% the real dimensions of the box.

- It was able to completing the production cycle and establishing a significant saving of 79.68% in terms of investment, since the overral cost of this machine is $ 1625.31 and a machine of the same dimensions and conditions in the market can cost up to $8000.0 depending on the brand and transportation taxes.

12. Recommendations

- Follow the instructions for installation and maintenance of the manufacturers of the elements purchased by catalogue.

- When using linear guides with already rectified bases, it is not necessary to rectify the surface where it will be installed, more to take into account the correct alignment so as not to suffer deformations of the base of the linear guide.

- It is recommended that the operator generate operation reports and maintenance of the CNC machine, to determine the times of cleaning and care according to the time of use of the same.

- The operating conditions must be ideal within the industrial environment, with a constant ambient temperature and constantly cleaning cardboard waste, this to

ensure that it does not interfere with the correct operation of both mechanical and electronic elements.

- The operation of the 4-axis CNC machine requires prior training for the operators, so that they know how it works and also to take into account all the safety precautions as it is a cutting machine.

- In order for the CAM and control software (GrblGru) to work optimally with 3D visualization, G-code generation and real-time G-code command monitoring, it is necessary to correctly select the 2D panel specifications for the generation of the G code with the ”tangential blade” job, ensuring in each job that the configuration is adequate for the type of material to be cut, on the other hand, in the 3D panel, the ”Macros” window must be handled correctly to ensure the proper position for the work of the product on the base.

- Between the bending and cutting subprocess, the material must not be displaced in any way, as well the vacuum suction must not be turned off, this to ensure that both bending and cutting are performed at the desired coordinates of the material.

- If it is faced a problem with a specific element of the CNC machine and in the event that the user manual does not satisfy all the required information needs, it is recommended to go directly to the technical manuals of the manufacturers.

REFERENCES

[1] R. Kerkaert, *Drag Tangential knife technology*. Summa, 2017.

[2] M. Ates, S. Karadag, A. A. Eker, y B. Eker, “Polyurethane foam materials and their industrial applications,” *Polymer International*, vol. 71, no. 10, pp. 1157–1163, 2022.

[3] “V-SLOT ALUMINIUM PROFILE C-BEAM 40X80 6MM SLOT - BLACK ANODIZED,” https://www.systeal.com/en/profiles-20-series/1581-v-slot-aluminium-profile-c-beam-40x80-6mm-slot-black-anodized.html, accessed: 2022-11-02.

[4] R. G. Budynas *et al.*, “Diseño en ingeniería mecánica de shigley,” 2012.

[5] “V-SLOT ALUMINIUM PROFILE 20X40 6MM SLOT- BLACK ANODIZED,” https://www.systeal.com/en/profiles-20-series/1581-v-slot-aluminium-profile-c-beam-40x80-6mm-slot-black-anodized.html, accessed: 2022-11-02.

[6] “Nema 17 Features,” https://components101.com/motors/nema17-stepper-motor, accessed: 2022-10-24.

[7] “Nema 23 Step motor M1233022,” https://www.lamtechnologies.com/Product.aspx-lng-ENidp-M1233022, accessed: 2022-8-18.

[8] G. Briere, *Grbl Mega 5x*. Github, 2018.

[9] “Aruco Marker,” https://arshren.medium.com/marker-based-augmented-reality-using-opencv-b851b82be4dc, accessed: 2022-11-02.

[10] T. Tocci, L. Capponi, y G. Rossi, “Aruco marker-based displacement measurement technique: uncertainty analysis,” *Engineering Research Express*, vol. 3, no. 3, p. 035032, 2021.

[11] M. Murariu y P. Dubois, “Pla composites: From production to properties,” *Advanced drug delivery reviews*, vol. 107, pp. 17–46, 2016.

[12] S. Pepsen, *WEAR RESISTANCE AND FRICTION COEFFICIENT OF POLYURETHANE*. Pep Polyutherane, 2020.

[13] F. P. Beer, E. R. Johnston, E. R. Eisenberg, y R. G. Sarubbi, *Mecánica vectorial para ingenieros*. McGraw-Hill, 1967, no. 968-422-565-2. 04-A1 LU. CG-12.

[14] T. Corp, *Aspiradoras y Abrillantadoras*, 2022.

[15] "VACUUM PUMPS," https://cncrouter.uk/mercury-vacuum-pumps.htm, accessed: 2022-11-02.

[16] "Aluminum 6063-T5," https://asm.matweb.com/search/MA6063T5, accessed: 2022-11-02.

[17] "Friction Coefficients," https://www.engineeringtoolbox.com/friction-coefficients-d$_7$78.$html, accessed : 2022 - 10 - 24.$

[18] J. E. Shigley y C. R. Mischke, *Mechanical engineering design (in SI units)*. Tata MacGrow Hill, 2006.

[19] "C-Beam," https://www.handsontec.com/dataspecs/Engineering%20Material/4080-C%20Beam.pdf, accessed: 2022-08-30.

[20] R. L. Mott, R. N. Salas, M. A. R. Flores, y E. B. Martínez, *Resistencia de materiales*. Pearson Educación, 2009, vol. 5.

[21] "Aluminium Extrusions," https://www.parker.com/content/dam/Parker-com/Literature/Electromechanical-North-America/CATALOGS-BROCHURES/IPS-Literature/IPS-Catalog-Parker-T-Slot-Aluminum-Profile-20200225.pdf, accessed: 2022-08-30.

[22] A. Calleja, P. Bo, H. González, M. Bartoň, y L. N. López de Lacalle, "Accurate 5-axis flank cnc machining with conical tools," *The International Journal of Advanced Manufacturing Technology*, vol. 97, no. 5, pp. 1605–1615, 2018.

[23] C. G. Martínez Romero, B. M. Pinzón Robayo *et al.*, "Automatización de una mesa de coordenadas xy para taladro fresador."

[24] N. Viswanathan, B. P. Krishnan, V. Vimala, B. Balaji, U. Praveenkumar, R. Sivapragadeesh, y G. Jayasuriya, "Experimental analysis of power consumption in cnc turning

centre for various chuck diameters," *Materials Today: Proceedings*, vol. 60, pp. 1409–1414, 2022.

[25] "Grbl-Mega-5X," https://github.com/fra589/grbl-Mega-5X, accessed: 2022-11-02.

[26] M. Marsono, Y. Yoto, A. Suyetno, y R. Nurmalasari, "Design and programming of 5 axis manipulator robot with grblgru open source software on preparing vocational students' robotic skills," *Journal of Robotics and Control (JRC)*, vol. 2, no. 6, pp. 539–545, 2021.

[27] "GrlBgru," https://www.grblgru.com/, accessed: 2022-06-13.

[28] M. Copeland, J. Soh, A. Puca, M. Manning, y D. Gollob, "Microsoft azure and cloud computing," in *Microsoft Azure*. Springer, 2015, pp. 3–26.

[29] M. Collier y R. Shahan, *Microsoft Azure Essentials-Fundamentals of Azure*. Microsoft Press, 2015.

[30] "Detection of ArUco Markers," https://docs.opencv.org/, accessed: 2022-11-02.

[31] B. Li, J. Wu, X. Tan, y B. Wang, "Aruco marker detection under occlusion using convolutional neural network," in *2020 5th International Conference on Automation, Control and Robotics Engineering (CACRE)*. IEEE, 2020, pp. 706–711.

[32] F. Pieterse y A. L. Nel, "The advantages of 3d printing in undergraduate mechanical engineering research," in *2016 IEEE Global Engineering Education Conference (EDUCON)*. IEEE, 2016, pp. 25–31.

[33] P. Feng, X. Meng, J.-F. Chen, y L. Ye, "Mechanical properties of structures 3d printed with cementitious powders," *Construction and Building Materials*, vol. 93, pp. 486–497, 2015.

[34] "La tarifa de energía eléctrica nacional," https://www.controlrecursosyenergia.gob.ec/las tarifas de energia electrica no se incrementaran en el 2022/::text=El%20Directorio%20de%20la%20Agencia,(%C2%A2USD%2FkWh), accessed: 2022-11-02.

[35] “How Much Power Does a 3D Printer Use?” https://www.clevercreations.org/how much electricity 3d printer power usage/, accessed: 2022-11-02.

[36] “Electricity Bill Calculation,” https://www.rapidtables.com/calc/electric/electricity-calculator.html, accessed: 2022-11-02.

[37] T. Gawroński, “Optimisation of cnc routing operations of wooden furniture parts,” *The International Journal of Advanced Manufacturing Technology*, vol. 67, no. 9, pp. 2259–2267, 2013.